



# Geomorphic Records along the General Carrera (Chile)–Buenos Aires (Argentina) Glacial Lake (46°-48°S), Climate Inferences, and Glacial Rebound for the Past 7–9ka

Jacques Bourgois, Maria Eugenia Cisternas, Regis Braucher, Didier Bourles,  
José Frutos

## ► To cite this version:

Jacques Bourgois, Maria Eugenia Cisternas, Regis Braucher, Didier Bourles, José Frutos. Geomorphic Records along the General Carrera (Chile)–Buenos Aires (Argentina) Glacial Lake (46°-48°S), Climate Inferences, and Glacial Rebound for the Past 7–9ka . *Journal of Geology*, 2016, 124 (1), pp.27-53. 10.1086/684252 . hal-01271536

**HAL Id: hal-01271536**

**<https://hal.science/hal-01271536>**

Submitted on 9 Feb 2016

**HAL** is a multi-disciplinary open access archive for the deposit and dissemination of scientific research documents, whether they are published or not. The documents may come from teaching and research institutions in France or abroad, or from public or private research centers.

L'archive ouverte pluridisciplinaire **HAL**, est destinée au dépôt et à la diffusion de documents scientifiques de niveau recherche, publiés ou non, émanant des établissements d'enseignement et de recherche français ou étrangers, des laboratoires publics ou privés.

# Geomorphic records along the General Carrera (Chile)-Buenos Aires (Argentina) glacial lake (46-48°S), climate inferences and glacial rebound for the past 7-9 ka

<sup>a,b,\*</sup>Jacques Bourgois, <sup>c</sup>Maria Eugenia Cisternas, <sup>d</sup>Régis Braucher, <sup>d</sup>Didier Bourlès, <sup>e</sup>Jose Frutos

<sup>a</sup>Sorbonne Universités, UPMC Univ Paris 06, UMR 7193, Institut des Sciences de la Terre Paris (iSTeP), F-75005, Paris, France. P: 33 (0)1 44 27 59 98; E-mail: [jacques.bourgois@upmc.fr](mailto:jacques.bourgois@upmc.fr)

<sup>b</sup>CNRS, UMR 7193, Paris, France.

<sup>c</sup>Instituto de Geologia Economica Aplicada (GEA), Universidad de Concepcion, Chile. P: 56 4 12 20 48 18; E-mail: [mcisternas@udec.cl](mailto:mcisternas@udec.cl)

<sup>d</sup>Aix-Marseille Université, CNRS-IRD-Collège de France, UM 34 CEREGE, Technopôle de l'Environnement Arbois-Méditerranée, BP80, 13545 Aix-en-Provence, France. P: 33 (0)4 42 97 15 09 ; E-mail: [braucher@cerege.fr](mailto:braucher@cerege.fr), P: 33 (0)4 42 97 15 16; E-mail: [bourles@cerege.fr](mailto:bourles@cerege.fr)

<sup>e</sup>Economic Geologist Consultant, San Juan de Luz 4060, Providencia, Santiago, Chile. P: 56 (0)9 89 00 74 00; E-mail: [frutosjg@gmail.com](mailto:frutosjg@gmail.com)

## Abstract

We present geomorphic, stratigraphic, and chronological data acquired along the General Carrera-Buenos Aires (GCBA) glacial lake located along a major morphological incision across the Andes. Complementing relevant available data, relative chronology of morpho-climatic records together with 18 <sup>10</sup>Be Cosmic Ray Exposure (CRE) ages allow constraining the timing of the Patagonian ice-sheet fluctuations since the LGM. It improves the knowledge of the Patagonia climate evolution in the 46-48°S area, and allows documenting the uplift rates (glacial rebound) for the past ~7-9 ka. The first major ice lobe retreat occurred after 17.3 ± 0.6 ka and has likely continued during the ACR from ~12.9 to 14.5 ka. Between ~12.9 ka and ~10.9 ± 1.3 ka, the General Carrera Lake evolved as an endorheic basin. Terraces T4 to T1 (top to bottom) have recorded abrupt lake regressions likely controlled by rainfall deficit. They have accumulated in the time interval ~17.3-12.3 ka (maximum limits). Two glacial readvances at ~10.9 ± 1.3 and ~7.9 ± 1.1 ka marked a major climate change that led the lake to be ice-dammed again. A major transgression occurred subsequently that have flooded the previously accumulated terraces. Since then, a pervasive regression has steered the GCBA

Lake to the situation at Present. The highest shoreline of the transgression is used as a passive marker in order to quantify the magnitude and character of the regional deformation. At 72°30' W, the GCBA Lake area uplifted (glacial rebound) at a rate between 15 to 33.5 mm.yr<sup>-1</sup> during the past  $7.9 \pm 1.1$  ka. We infer that the high uplift rate mainly originates from the North Patagonian icefield ice loss.

**Keywords:** Patagonia, General Carrera Lake (Chile), Buenos Aires Lake (Argentina), Morphology, Stratigraphy, Chronology, Cosmic Ray Exposure ages, Last Glacial Maximum, Holocene, Climate inferences, Isostatic rebound, Slab window.

## 1. Introduction

The N-S trending Andes separating the Pacific Ocean to the West from the foreland lowlands to the East dominate the topography of Patagonia. An elongated ice sheet, the Patagonian ice sheet (Fig. 1), extending over 1800 km between 38° and 56°S covered the high relief of this major mountain belt (Kaplan et al., 2004; Sugden et al., 2002; Lowell et al., 1995; Hulton et al., 1994) during the Last Glacial Maximum (LGM) at ~19-29 ka (Boex et al., 2013; Hein et al., 2009; Douglass et al., 2006; Kaplan et al., 2004; Singer et al., 2000; Fleming et al., 1998). The North and the South Patagonian icefields (NPI and SPI, respectively) are today restricted remnants of the maximum glacier extent. At Present, these Patagonian icefields are the largest glaciers in the southern hemisphere outside of Antarctica.

At 46-48°S the GCBA Lake is the trace of a major ice lobe that originated from the NPI (Fig. 2). Moraine markings provide record of ice retreat since the LGM (Glasser et al., 2012; Kaplan et al., 2011; Moreno et al., 2009; Kaplan et al., 2004; Wenzens, 1999; Clapperton, 1997; Marden and Clapperton, 1995; Markgraf et al., 1992; Mercer, 1982). At Present the GCBA Lake flows to the Pacific Ocean bypassing the Andes crest line at ~2000-4000 m through the Rio Baker. Because a thick ice sheet covered the Andes during maximum ice extent melt water had to stream eastward through the Rio Deseado that drained the Andes to the Atlantic Ocean during the LGM and part of the subsequent deglaciation. In this study we investigate the ice retreat history and water level fluctuations along the GCBA Lake for the past ~27-29 ka with special reference for the past ~15-17 ka following the last main ice lobe development. We use the in-situ produced <sup>10</sup>Be cosmogenic nuclide to determine the CRE ages of samples from boulders located at moraine crests, drop-stones on terraces, and preserved glacial polish on bedrock. The CRE ages of dropstones resting on strandlines and

terraces allowed us to reconstruct confidently the GCBA Lake evolution, outlet routing, and history during the LGIT and the Holocene that complement the pioneer studies by Bell (2008) and Turner et al. (2005). The evolution of the GCBA Lake area provides constraints on the vertical isostatic adjustment (i.e. rebound) driven by ice decay and ice volume loss for the past 7-9 ka.

## **2. Background**

### **2.1. Geologic setting**

The studied area (45-48°S) is located at the latitude of the Chile triple junction area (Fig. 1) where the Antarctica, the Nazca, and the South America plates meet (Bourgois et al. 2000; Behrmann et al., 1992; Leslie, 1986; Cande and Leslie, 1986). At 46°09'S, the active spreading center at the Antarctic-Nazca plate boundary –i.e. the Chile ridge– is being subducted beneath the South America continental margin. When a spreading ridge intersects a subduction zone, the diverging oceanic plate edges become surrounded by hot mantle, a slab window develops at depth (Dickinson and Snyder, 1979; DeLong et al., 1978). At the studied area, the Patagonian slab window extends beneath the GCBA Lake area at depth (Russo et al., 2012; Breitsprecher and Thorkelson, 2009; Bourgois and Michaud, 2002). The GCBA Lake area is slab-free (Gorring and Kay, 2001; Gorring et al., 1997). Plio-Pleistocene basalts that erupted along this area at the Meseta del Lago Buenos-Aires provide evidence for asthenosphere-lithosphere interaction during slab window development (Orihashi et al., 2013; Guivel et al., 2006; Gorring et al., 2003; Gorring and Kay, 2001). This situation has an impact on the mechanical strength properties of the Patagonia lithosphere and upper mantle that in turn must induce a signature on the rate of vertical crustal motion (rebound) associated with ice mass loss.

The Andean batholith of Cretaceous to Lower Miocene age (SERNAGEOMIN, 2002) is a major rock unit of the Patagonia Andes. Along the studied transect, it extends from the Bertrand Lake to the east to the Pacific coastline to the west intruding metamorphic complexes over a distance of more than 100 km. The major component of the moraines and drop-stones from the GCBA ice lobe are granitic rock from the Patagonian batholith.

### **2.2. Paleoclimatic background**



106

107       The 3 to 4 km high Patagonian Andes form a prominent topographic barrier to the  
108 Westerlies atmospheric circulation in the southern hemisphere and cause one of the most  
109 pronounced orographic rain shadow on Earth. Between 46° and 49°S rainfall along the Pacific  
110 western slopes is  $>3000 \text{ mm.yr}^{-1}$ ,  $\sim 10$  times higher than along the eastern side of the  
111 Argentina Andean foreland (Hoffman, 1975). The Pacific Ocean to the west, together with the  
112 Andean Cordillera with peaks rising above 3000 m and the dry steppes of Argentina in the  
113 rain shadow of the Andes to the east control the climate of Patagonia. The cool temperate belt  
114 extends south of 42°S (Miller, 1976) while the Westerlies and precipitation reach a maximum  
115 at around 50°S where the mean annual precipitation may exceed 5000 mm at sea level.  
116 Precipitation totals decrease sharply northward from 2000 mm at 40°S to  $<150 \text{ mm}$  at 30°S  
117 (Hoffman, 1975). Numerical modeling aiming to reconstruct the climate of Patagonia during  
118 the LGM (Hulton et al., 1994) shows a northward migration of precipitation belt of  $\sim 5^\circ$  (Fig.  
119 1) with a decrease of the annual precipitation totals at 50°S and an increase at 40°S, the  
120 Westerlies reaching a maximum at 45°S. The topographic barrier of the Andes is expected to  
121 influence the atmospheric circulation similarly during both glacial and interglacial periods.

122

### 123 2.3. Timing of ice retreat

124

125       In the GCBA Lake area, the maximum extent of the LGM ice lobe occurred between  $\sim 25$   
126 and 29 ka (Boex et al., 2013; Hein et al., 2010). This is in agreement with the glacial  
127 maximum at 26-27 ka B.P. identified at the Lago Llanquihue piedmont lobe (Lowell et al.,  
128 1995) located several hundreds of km to the north. The LGM and the subsequent retreat of the  
129 GCBA ice lobe is marked by a large moraine system located at 150-200 km east of the NPI  
130 (Singer et al., 2000; Kaplan et al., 2004; Douglass et al., 2006; Hein et al., 2009). Based on  
131 paired  $^{10}\text{Be}$  and  $^{26}\text{Al}$  ages, Kaplan et al. (2004) have first identified the youngest  
132 Fenix/Menucos moraine complex at the Perito Moreno outlet area with ages ranging from  
133  $22.9 \pm 1.3$  to  $15.1 \pm 0.5$  ka. Subsequently, the in-situ produced  $^{10}\text{Be}$  production rate,  $^{10}\text{Be}$  half-  
134 life and muonic production parameters have been dramatically revised (Blard et al., 2013;  
135 Kelly et al., 2014; Braucher et al., 2011; Chmeleff et al., 2010, Korschinek et al., 2010). This  
136 implies that all CRE ages published before 2010 are systematically underestimated by at least  
137 28% considering in addition that the  $^{10}\text{Be}$  half-life they used is  $\sim 9\%$  higher than the recently  
138 re-evaluated one. Kaplan et al. (2011) have re-calculated the Fenix I to V and the Menucos

moraine ages using updated parameters close to those accepted at present. They have documented the following mid point ages for the Menucos and Fenix I to V terminal moraines: Menucos ( $17.3 \pm 0.6$  ka), Fenix I ( $18.5 \pm 0.8$  ka), Fenix II ( $19.8 \pm 0.6$  ka), Fenix III ( $21.8 \pm 0.7$  ka), Fenix IV ( $26.3 \pm 0.9$  ka), Fenix V ( $25.7 \pm 0.9$  ka). Therefore, the timing of the onset of massive deglaciation has occurred between 16.7 and 17.8 ka, after the last re-advance or still stand of the ice lobe recorded by the Menucos Moraine. However, this re-calculated  $^{10}\text{Be}$  ages from Kaplan (2011) conflict the previous description by Kaplan et al. (2004). Indeed they have shown that the youngest Menucos moraine is overlying lake sediment dated at  $15.5 \pm 0.5$  cal ka (AMS radiocarbon age). Consequently, the age of the last major ice re-advance must be younger than 15 to 16 ka. This opens the question of the attribution of this moraine to the Menucos moraine. A re-advance of the GCBA ice lobe that would be younger than the Menucos moraine may exist in the Perito Moreno outlet area. Recently, Boex et al. (2013) have presented a reconstruction of the Patagonia ice-sheet evolution from the LGM. They considered that the ice-sheet profile has remained extensive and close to its LGM extent until  $\sim 19$  ka. Rapid ice-sheet thinning initiated at 18.1 ka reaching its present dimension at 15.5 ka. The outcomes from Boex et al. (2013) are conflicting with those from Kaplan et al. (2011 and 2004) with a gap of  $\sim 150$  km in ice extent during the same time window, along the same area. Also, Boex et al. (2013) claim that no substantial ice re-advance has occurred during the Antarctic Cold Reversal (ACR) and the Younger Dryas (YD).

To document paleoclimat changes during the LGIT, a palynological record from the Guanaco Lake (Torres del Paine area) was developed (Moreno et al., 2009). The obtained record documents dominance of pre-Andean herbs and shrubs between 11.4 and 12.5 ka and a rapid increase in *Nothofagus* ca. 12.3 ka that document the onset of massive ice recession at ca. 12.6 ka at about  $50^\circ\text{S}$ .

In the study area, published data reveal contradictions. In this work, the accepted assumptions and ages are as follow: (1) a major re-advance of the GCBA ice lobe occurred at 15 to 16 ka, the major ice recession has to occur subsequently; (2) ages for the YD (11.5 to 12.8 ka) and the Antarctic Cold Reversal (ACR, 12.9 to 14.5 ka) are those from Jomelli et al. (2014) that use the most recent updated production rates for cosmogenic  $^{10}\text{Be}$  and  $^3\text{He}$ ; (3) the onset of massive ice recession occurred at  $\sim 12.6$  ka.

## 2.4. GCBA Lake evolution

The E-W trending GCBA Lake is 585 m deep (Murdie et al., 1999) and 130 km long extending ~ 55 km eastward across the Andean foreland. To the west, the Rio Baker —i.e. the outlet of the GCBA Lake, water level at 201 m— streams between the disconnected NPI and SPI (3-4 km in elevation), until reaching the Pacific. At Present the drainage divide (392 m at Perito Moreno) is located along the Fenix moraine system at the eastern ends of the GCBA Lake. During the LGM a continuous ice sheet blocked the route to the Pacific causing meltwater from the GCBA ice lobe to drain to the Atlantic. After 15-16 ka, deglaciation results in a drainage diversion as the ice disintegrated in the Andes (Hein et al., 2010; Bell, 2008; Turner et al., 2005; Bourgois et al., 2000; Mercer, 1976; Caldenius, 1932). During the LGIT, cold events such as the ACR, the Younger Dryas, and the subsequent 8.2 ka Cold Event, major glaciers including those from tributaries of the Rio Baker potentially dammed the water outflow to the Pacific (Boex et al., 2013; Hein et al., 2010; Bell, 2008; Glasser et al., 2005; Turner et al., 2005) resulting in ice-dammed paleolake formation. Geologic evidence indicates the presence of such paleolakes at heights ranging from about 100 m to about 330 m above the present-day elevation of the GCBA Lake. Evidence includes paleoshorelines, beaches, terraces, raised deltas, and lake sediments (Bell, 2008; Douglass et al., 2005; Turner et al., 2005; Wenzens, 2005; Caldenius, 1932).

Turner et al. (2005) have described the GCBA Lake fan-deltas and terraces through the concept of the “United Lake”, which closely associates the GCBA (201 m in elevation at Present) and the Cochrane-Pueyrredon (CP, 152 m in elevation at Present, Fig.1) Lakes evolution. The routing of the “United Lake” water to the Atlantic occurred through the Rio Deseado. Using 16 ages, 15 of them being located outside the GCBA Lake, they reported the development of two paleolake shorelines along the GCBA Lake. Mollusc shells sampled along a terrace (315 m in elevation, lower paleolake shoreline) located at the Chile Chico Mirador have provided a cosmogenic calibrated age of  $13.5 \pm 0.2$  ka. Subsequently, Hein et al. (2010) developed a model based on the “United Lake” concept. They have proposed an evolution through two steps, the Upper United-paleolake (fan delta at 370-400 m in elevation) and the Lower United-paleolake (fan delta at 300-270 m in elevation) steps, both occurring in the time interval 15-16.5 ka.

From a detail study of the Rio de Las Dunas area (GCBA Lake), Bell (2008) has conducted a focused analysis on the paleolake levels. Bell (2008) identifies a series of seven raised lacustrine braided deltas at elevations ranging from 100 to 450 m above Lago General Carrera i.e. ~300 to 650 m amsl. The deltas were formed by the punctuated drainage of a paleolake called the “Predecessor Lake” —i.e. the two GCBA-CP connected lakes—. Breaking of ice

dam would have caused the “Predecessor Lake” to drop abruptly by 30 to 150 m, which was followed by periods of stability. A volcanic ash layer covering the Bell’s “Delta 2”—i.e. equivalent to the Lower United-paleolake of Turner et al. (2005)— was ascribed to a 6.7 ka BP eruption of Volcan Hudson (Bell, 2008). If this interpretation is correct, it provides a benchmark age for the Deltas 2 and 1, which are older and younger than 6.7 ka, respectively. Also, Bell (2008) suggests that the Delta 1 was still in existence at this time in the Holocene. Bell (2008) considers that the punctuated drainage of the “Predecessor Lake” as recorded by Deltas 1 to 7 began at ~13 ka ago.

### 3. Methods

#### 3.1. Geomorphic imprints

Three main geomorphic features have recorded the morpho-climatic and tectonic evolution of the studied area. These signatures include moraines at the glacial lobe terminations, fan-deltas built by stream-transported sediments to the GCBA Lake, and a dense flight of strandlines. The strandline sequence documented throughout the GCBA Lake area exhibits a pervasive signature. Regarding the direct action of glaciers, terminal moraines have mainly been sampled east of the GCBA Lake. These moraines have recorded major stages of ice lobe re-advances and related paleo-environmental conditions from the LGM to the ACR.

At Present, fan deltas or terraces (Fig. 3) are especially developed along the General Carrera Lake (Chile). Bell (2008) and Turner et al. (2005) have described the GCBA Lake fan-deltas and terraces through the concept of the “Predecessor Lake” and the “United Lake” concepts (see section 2.4.), respectively. Because no age and elevation correlations for fan deltas and terraces of the GCBA and CP Lakes is consistently documented, the present work proposes direct elevation measurements and ages for the GCBA Lake fan deltas.

As soon as the water of a stream encounters the standing water of a lake, speed drops rapidly, which leads to the development of a fan-delta from load deposit. An evolving fan-delta is recording the evolution of the lake level through time. Also, the accumulated sediments display evidences of highly variable currents and changes of facies. The braid deltas built into the GCBA Lake display topset, foreset, and bottom layers showing a typical Gilbert Delta organization (Fig. 3D). These geomorphic imprints were described in great details by Bell (2008). Between 201 m —the lake level elevation at Present— and ~ 530 m,

the northern and the southern banks of the General Carrera Lake exhibit five main levels, T4 to T0 of such fan deltas or terraces (Fig. 3A, B, C, E, and F). Based on a precise mapping of the Rio de Las Dunas area (Bell, 2008), terraces were labeled 7 to 1 from top to bottom. Terraces T4, T3, T2, T1, T0 (top to bottom) identified in this work match the Bell's terraces 5, 4, 3, 2 and 1, respectively. The Bell's terraces 7 and 6 are considered as river terraces in this work. Another major record of the evolution of the lake water level is the strandline sequences underline by notches and wave-cut terraces (Fig. 4A to D). The major terraces identified all around the GCBA Lake connect laterally to strongly notched strandlines. These sequential records, including fan deltas and strandlines, have left in the landscape a strong imprint that underlines the main water level stages. Frequently, a tempestite barrier (Fig. 4A) underlines the coastline at Present. The tempestite records were identified not only along beaches (Fig. 4B) but also at the fan delta front (Fig. 4A) along the shoreline documenting the recent water level lake evolution. The morphologic analysis of the older terraces —i.e. old fan-deltas— shows that such tempestite records exist along the paleo-shorelines. The terraces of the GCBA Lake area exhibit isolated erratic boulders (dropstones) left on terraces (Fig. 5A to D). The dropstone emplacement that post-dates the terrace accumulation allows constraining the lake level evolution, and age during the GCBA ice lobe retreat during the LGIT. The above listed morphologic features and age are used to disentangle the chronology of the GCBA Lake evolution. However, the lake size, the evolution of the potential outlets, and the glacial isostatic rebound make the approach difficult.

### 3.2. Sampling procedure and method

Sampling sites (Fig. 2) are located along the GCBA Lake between 70°30' and 73°50'W, from the eastern foreland of the Andes to the Rio Baker River outlet. All the dated samples but the glacial polish (sample 25, Table 1) originated from granite boulders comprising from 15 to 30% quartz. The local geological background consists in a metamorphic basement covered by volcanic and sedimentary rocks that differ from the sampled blocks. The sampled blocks originated from the Patagonian batholith located 50 to 200 km west from their current location. The GCBA ice lobe and icebergs originating from the NPI during the subsequent pro glacial phases of the lake transported them. Our sampling selection strategy has been established to minimize the effects of pre-exposure prior to exposition and of denudation following deposition. Samples were collected by hand with hammer and chisel from the tops

of boulders as close to the center of the upper surface as away from the edges as possible. Preference was given to large —i.e. more than 1.5 m in diameter—, flat topped and stable boulders. Only the top 2 to 5 cm of the selected boulders was sampled. The location (Fig. 2), the age (Table 1) and elevation (Table 2) of each boulder and morphologic features were surveyed using two TRIMBLE 4600 LS receivers in association with a hand-held global positioning system (GPS) for lateral correlation. The vertical location of the upper part of terraces and paleo-shoreline locations are the main error source. The accuracy of the field leveling carried out is estimated to be at worst  $\pm 5$  m. Elevation was further controlled plotting the sample locations on topographic maps. The estimated horizontal accuracy is better than 3-4 m.

### 3.3. Cosmogenic surface exposure dating

CRE dating is based on the quantification of the cosmogenic nuclide content accumulated in a rock exposed at the surface to cosmic rays. This high-energy cosmic radiation induces a nuclear reaction when penetrating Earth's environment (Lal, 1991 a and b). Energetic particles interact with target atoms to produce cosmogenic nuclides. Eighteen samples (Fig. 2, Table 1) have been collected from key sites. Quartz was isolated and purified from the atmospheric  $^{10}\text{Be}$  following the standard method (Merchel and Herpers, 1999; Brown et al., 1992). After dissolution in Suprapur HF, the resulting solution was spiked with 300  $\mu\text{g}$  of  $^9\text{Be}$  carrier (Brown et al., 1991). Beryllium was extracted (Brown et al., 1992; Bourlès, 1988), and cosmogenic  $^{10}\text{Be}$  measurements were performed with the AMS Tandetron facility (Gif-sur-Yvette, France) (Raisbeck et al., 1987, 1994). The measured  $^{10}\text{Be}/^9\text{Be}$  ratios were corrected for procedural blanks and calibrated against the National Institute of Standards and Technology standard reference material 4325 by using an assigned value of  $2.79 \pm 0.03 \times 10^{-11}$  and a  $^{10}\text{Be}$  half-life of  $1.387 \pm 0.012 \times 10^6$  years (Korschinek et al., 2010; Chmeleff et al., 2010). Analytical uncertainties (reported as  $1\sigma$ ) include uncertainties associated with AMS counting statistics, procedural blank measurements ( $^{10}\text{Be}/^9\text{Be} = 4.372 \pm 2.524 \times 10^{-15}$ ) and the AMS internal error (3%). A sea level, high-latitude (SLHL) spallation production of  $3.67 \pm 0.17 \text{ at.g}^{-1}.\text{yr}^{-1}$  calibrated against  $^3\text{He}$  in the Tropical Andes (Blard et al., 2013) was used and scaled for latitude (Stone, 2000) and elevation. The contribution of muons to the production rate was calculated using the physical parameters recently re-evaluated by Braucher et al. (2011). Because it uses updated physical parameter, the  $^{10}\text{Be}$  production rate used in this work

is more accurate as compared to that at  $3.71 \pm 0.11 \text{ at.g}^{-1}.\text{yr}^{-1}$  proposed by Kaplan et al. (2011). However, the  $^{10}\text{Be}$  production rate calculated by Kaplan et al. (2011) in an area located few hundreds of km south of the studied area overlaps that retained in this work. Therefore, no re-calculation is done regarding the ages provided by Kaplan et al. (2011, supplementary material) for the Menucos and Fenix moraines.

Because the concentration of in situ produced cosmogenic nuclides depends both on the exposure duration to cosmic rays and on the denudation rate, CRE ages can be calculated only if the relevant denudation rate is known or can be neglected. All minimum CRE ages presented (Table 1) are calculated neglecting denudation, which is justified in our case for most of the discussed samples considering the maximum denudation rates calculated from the samples having reached steady-state ( $0.049 \pm 0.02$  and  $1.31 \pm 0.16 \text{ m/Ma}$  for samples 4 and 17 (Table1), respectively and the short time interval investigated that extends at most over the last 40 ka. Vegetation is limited to small shrubs and historical snow accumulation has been thin and short-lived in this semi-arid area (Garreaud et al., 2013). Moreover, climate models suggest that aridity increased during colder periods (Hulton et al. 2002).

## 4. Results

### 4.1. Buenos Aires Lake area

Two samples (15 and 69, Fig. 6 and 7) were collected along the Menucos and the Fenix I moraine crests. The  $^{10}\text{Be}$  analyses (Table 1) yield to minimum ages of  $20.5 \pm 8.4$  and  $20.2 \pm 2.6 \text{ ka}$ , respectively. Although imprecise, these values are remarkably similar.

Between the current lake level at 201 m and  $415 \pm 5 \text{ m}$  elevation, the Buenos Aires Lake northern rim exhibits a pervasive flight of strandlines (Fig. 8). These regressive parallel strandlines have recorded the complex lake level evolution through time, as it was free of ice. Above  $415 \pm 5 \text{ m}$  elevation, the shore area exhibits several steps characterized by flat parallel strips bounded lakeward by steep side. The flat strips, which exhibit a braided pattern of meander loop, are outwash plains covered by well-rounded conglomerates. The arcuated steep side follows the inner side of the arcuated ridges previously constructed during moraine accumulation. The essential factors for braiding are bed-load sediment transport and laterally unconstrained free-surface flow, conditions that characterize the lateral evolution of a retreating ice lobe. The arcuated moraine succession controls the subsequent evolution of

braided pattern strips. The arcuated moraine ridges have recorded re-advance or still-stand of ice lobe during cold episodes whereas braided pattern evolved subsequently during ice lobe retreat during warmer episodes. Towards the lake, the morphologic signature evolves abruptly to an area characterized by parallel regressive strandlines. In this study, we consider that the Buenos Aires Lake began to be free of ice after the Menucos glacial event. Since then, the evolution to the free-of-ice situation occurred during the ACR (see previous section). Subsequently, the lake water level was fluctuating between elevations ranging from  $415 \pm 5$  to 201 m, mainly controlled by the Bertrand/Baker spillway and rainfall. Along the northern rim of the lake the arcuated moraine pattern controlled the stream drainage. At Present, the Rio Fenix Grande is streaming eastward following the pre-existing moraine/braided pattern morphology.

## 4.2. Chile Chico area

Sample 23 (Fig. 7) was collected along a perched lateral moraine located west of Chile Chico at ~1116 m amsl. Its  $^{10}\text{Be}$  concentration yields to a minimum CRE age of  $34.2 \pm 10.4$  ka (Table 1). The moraine lies on a flat area at less than 10-15 m away from the slope break along the sub-vertical flank of the main U-shaped glacial valley —i.e. the ice edge at the time accumulation of the lateral moraine during the ice growth optimum during the LGM—. Because the GCBA Lake at Present is more than 400 m deep (Murdie et al., 1999), the estimated thickness of ice along the GCBA lobe at the longitude of sample 23 was ~1.5 to 1.7 km during the LGM.

Coupled climate/ice sheet models were developed in order to simulate the inception and growth of the Patagonia ice sheet (Klemann et al., 2007; Sugden et al., 2002; Ivins and James 1999; Hulton and Sugden, 1997). These models simulate the altitude evolution of the snowline through time. The equilibrium-line altitude (ELA) or snowline (Bakke and Nesje, 2011) is the average elevation of the zone where snow accumulation equals ice ablation over a one-year period. Although the ELA is determined by local weather conditions, it is a good proxy of regional climate conditions because glacier mass-balance fluctuations are correlated over distances of ~500 km. At the local and regional scale of the NPI, the ELA position allowed estimating the ice area change (Rivera et al., 2007; Aniya et al., 1996). While the Present ELA position can be determined without major difficulties, collecting relevant data for reconstructing past ice cap evolution remains challenging. Although sometimes



questioned, lateral moraines are regarded as reflecting the corresponding ELA since lateral moraines are considered to deposit only in the ablation zone below the ELA. Considered as relevant for lengthy ice lobe, this widely accepted method might provide confident information along the GCBA glacial lake.

Therefore sample 23 provides an estimate for the ELA during the LGM. At that time the ELA was at ~1100 m above sea level (no rebound correction), an elevation similar to that proposed for the Chilean Lakes region during the LGM (Porter, 1981). At Present, the ELA along the eastern side of NPI is 1350 m (Aniya, 1988; Casassa, 1987) —i.e. ~250 m (minimum value) higher than during the LGM—.

### 4.3. Fachinal area

Douglass et al. (2005) have studied in great detail the Fachinal area (Fig. 2 for location). At the outlet of the Rio Aviles they have identified two different moraines documenting two ice lobe advances during the Holocene recorded by an Outer and an Inner moraines with ages at  $8.5 \pm 0.7$  ka and  $6.2 \pm 0.8$  ka, respectively. These two moraines provide constraint for age accumulation of the underlying T1 terrace, which must be older than the older moraine. In this specific area, the T1 terrace is 314 to 293 m in elevation. Two km northeast of Fachinal, along the northern rim of the General Carrera Lake is the Rio Avellano fan-complex and terraces. At this site, the T0 and T1 terraces exhibit elevations similar to those of Fachinal. Unlike the Fachinal area, the Rio Avellano outlet area shows the development of a T2 terrace with elevation ranging from 391 to 413 m.

Because the basic work by Douglass et al. (2005) is a key point not only in itself but also in placing a major step in the climate and geomorphic evolution of the GCBA Lake area, we have re-calculated the Fachinal moraine ages using updated parameters (see sections 2.3 and 3.3). The new proposed ages are  $10.9 \pm 1.3$  and  $7.9 \pm 1.1$  ka for the Outer and the Inner moraines, respectively (Fig. 6). Therefore the T1 terrace accumulated before  $10.9 \pm 1.3$  ka.

### 4.4. Rio de Las Dunas, Rio Las Horquetas and Rio Los Maitenes area

Between 201 and 528 m in elevation, the outlet areas of the Rio de Las Dunas, Rio Las Horquetas and Rio Los Maitenes exhibit five major terraces, T0 to T4 from base to top (Fig. 9). This area was described in details by Bell (2008). The most recent T0 terrace, still

evolving as a fan-delta at Present, exhibits elevation ranging from 201 to 228 m. At Rio de Las Dunas outlet, the T0 terrace protruding northward toward the lake connects eastward to a sequence of 12-15 strandlines —i.e. paleoshore lines—, which developed between 201 and 211 m along a small embayment (Y1, Fig. 4 C). One to two meters high tempestite barriers underline the most prominent strandlines. As the lake level drop down, the fan-delta —i.e. the so-called T0 terrace— and laterally connected strandlines develop. The association between sediment accumulation at fan-delta and regressive strandlines strongly suggests that no major rupture in the lake level evolution have occurred during these two coeval morphogenic processes. Two potential factors, including decline in precipitation and bedrock incision at the Rio Bertrand outlet spillway, controlled the lake level drop from 211 to 201 m. Because ice damming occurred along the GCBA Lake spillway, during T1 to T4 terraces accumulation, we infer that the climate —i.e. rainfall deficit— is also responsible for the lake level variations during the time period from the ACR to  $10.9 \pm 1.3$  ka.

The elevation of the T1 terrace ranges from 302 to 347 m. This main terrace (Fig. 9 A and B) shows a major development along the General Carrera Lake. Due to the fact that the terrace (Fig. 3F) exhibits deeply notched strandline in its along-shore prolongation, especially in the Pto Guadal area. We infer that it develops during a fairly long time period of stable climate conditions. The T1 terrace cliff exhibits a deep incised valley (point X, Fig. 9 A and B) in which 65 m of sediment accumulated after incision. Because the T0 terrace accumulation post-dates the infill of the valley at point X, a transgression phase has occurred between the T0 and T1 terraces accumulation. South of the Rio de Las Dunas mouth, the T1 terrace cliff (point Y3, Fig. 10) exhibits a dense flight of strandlines (point Y3, Fig. 4 C) with a signature similar to those left from tempestites described at the embayment shown at Figure 4 C (see above). As documented at point X (Fig. 9 A and B), lake reoccupation occurred with water level rising to the top of the T1 terrace cliff, at least.

The T2 terrace is 432 to 468 m in elevation. Along the eastern bank of the Rio de Las Dunas a major flight of strandlines has left a pervasive imprint on the T2 terrace that connects upslope to the area occupied by the T3 terrace. The cliff bounding the T3 terrace downslope is partly removed by subsequent lake reoccupation and associated shoreline erosion. The T2 terrace connects southwestward to a deeply notched strandline (Fig. 3 F). The sample 59 from a dropstone lying on the strandline yields a minimum CRE age of  $15.0 \pm 1.8$  ka (Table 1) that constrains the minimum T2 terrace age. The T3 and T4 terraces are 472 to 495 and 499 to 528 m in elevation, respectively. As opposed to the lower terraces —i.e. T0 and T1— described above, the T3 and T4 terraces exist only in the Rio de Las Dunas and Rio de Los Maitenes

embayment area. This area exposed to prevailing wind direction exhibits a large amount of dropstones resulting from drifting of icebergs toward this trapping zone. We infer that the T3 and T4 terraces accumulated in an ice-wall lake environment. A large ice lobe was still flowing along the General Carrera Lake at that time. Five dropstones were sampled in this area. The 10 x 6 m granite block (sample 31, Fig. 5 B) on top the T3 terrace (location Fig. 9 B) yields a minimum CRE age of  $16.5 \pm 4.1$  ka (Table 1). Two dropstones, samples 61 and 71 on top of the T4 terrace yield minimum CRE ages of  $15.2 \pm 3.7$  and  $18.8 \pm 3.9$  ka, respectively. To the southwest, in the prolongation of the T4 terrace, sample 57 (Fig. 9 B, Table 1) from a dropstone (Fig. 5 D) located few meters below the uppermost strandline identified along the General Carrera Lake, yields a minimum age of  $18.5 \pm 3.7$  ka. Terraces T3 and T4 exhibit extensive flights of strandlines extending from  $\sim 527$  m in elevation in the area of Rio de Las Dunas to less than 325 m east of Rio Los Maitenes (Fig. 9 B). The imprint of each single strandline and their association as flight exhibits a signature similar to the tempestite flights identified along T0, T1, and T2 terraces (see above). These morpho-climatic imprints document a major phase of transgression, up to the T4 terrace, followed by a retreat of water as recorded across terraces T4 to T1. The sample 73 (Fig. 4 D, 9 B) collected on top the upper tempestite strandline, which notches the T4 terrace at about 521 m elevation, yields a minimum CRE age at  $9.9 \pm 2.5$  ka, significantly younger than dropstones sampled on top T3 and T4 terraces.

#### 4.5. Rio Müller area

The Rio Müller (Fig. 11) is located north of the General Carrera Lake. The lake shoreline east of Bahia Murta (Fig. 2) and its eastward prolongation towards the outlet of the Rio Müller display a pervasive development of terraces T0, T1 and T2 with elevation ranging from 201 to 227, 302 to 334, and 413 to 448 m, respectively. These elevations are consistent to those recorded south of the lake at the same longitude. As at other locations (Fig. 3 D), the Rio Müller outlet area exhibits along the northern rim of the lake an incision of the T1 and T2 terraces (Fig. 11 B, C) that deeply involves the metamorphic basement rock. Elevation measurements at the surveyed area (Fig. 11 A, B, C) have documented a  $\sim 94$  m incision (Fig. 11 D) occurring after the T1 and T2 terrace accumulation. Because  $\sim 102$  m of basement incision occurred after deposition of the T1 terrace accumulation at the Rio El Salto area (Fig. 3 D), we infer a similar situation at the Rio Müller. At this site, most of basement incision is

postdating the accumulation of the T1 terrace. As exemplified at Pto Ingeniero Ibañez and Rio de Los Maitenes areas (Fig. 7 and 9, respectively) the basement incision identified at different sites along the General Carrera Lake mainly occurred after the accumulation of the T1 terrace.

#### 4.6. Western outlet area

At Present time, the General Carrera Lake flows to the Pacific Ocean through the Lago Bertrand, which connects downstream to the Rio Baker. This simple draining route shows a complex evolution through time (Glasser et al., 2012) involving the Lago Negro, the Lago Bertrand, the Rio Bertrand, the Lago Plomo and the Rio Baker spillways (Fig. 12 and 13).

At the El Martillo area (Fig. 12 A, B), the General Carrera Lake is actively outflowing westward to the Lago Bertrand. The channel connecting the General Carrera Lake to the Lago Bertrand erodes ~100 m of the basement rock underlying a moraine ridge cropping out at 300 to 450 m elevation. Samples 45 and 49 from the moraine (Fig. 12 B and Table 1) yield minimum CRE ages of  $17.5 \pm 3.7$  ka and  $20.0 \pm 2.9$  ka, respectively. Northeast of the channel the General Carrera shoreline area exhibits the moraine overlaying fan-delta sediment. At this site the moraine has removed the upper part of the terrace. However, the internal bedding of the terrace documents delta growth towards the General Carrera Lake. We infer that the Lago Bertrand outlet was flowing eastward, in opposite direction as compared to the situation at Present. Strandlines notch deeply the moraine ridge documenting subsequent flooding. Finally, drainage to the west has induced ~100 m incision of the channel spillway to Lago Bertrand.

The Lago Negro (Fig. 13) with water level at ~ 235 m elevation shows no outlet at Present. To the west, a bare rock dome of metamorphic rock prevents connection with the Lago Bertrand. This metamorphic basement exhibits large –i.e. hundred of meters long– drumlins documenting ice flow to the east. East of Lago Negro, a ~ 30 to 100 m high moraine ridge obstructs the pathway towards the General Carrera Lake. A  $^{10}\text{Be}$  mean age of  $11.2 \pm 1.3$  ka for three samples has been documented for this moraine (Glasser et al., 2012) suggesting that the ice lobe re-advance at this site occurred during the YD. This moraine unconformably overlies a thick fan-delta accumulation (Fig. 13 B and D) displaying foreset layers dipping towards the General Carrera Lake –i.e. to the NE–. Because the moraine has abraded most of the fan-delta topset layers, no precise elevation of the upper part of the corresponding terrace is known. However, a minimum elevation of ~300 m is documented that allows us to assign

the fan-delta to the T1 terrace episode. A thick T1 terrace accumulation located along the southern rim of the Lago Negro corroborates this assumption (sampling site 39, Fig. 13 A). This terrace showing a well-preserved topset layers at ~364 m (highest elevation) exhibits several dropstones. One of them (Fig. 5 C) yields a minimum CRE age of  $14.4 \pm 3.0$  ka (sample 39, Table 1). Northwest of the Lago Negro moraine (Fig. 13 A and C) pervasive strandlines exist between 300 and 400 m elevation. The lower strandlines notch the moraine that documents a fluctuating lake level and a subsequent flooding of the moraine. Northwest of the main moraine outcrop (Fig. 13 A and B) a morphological depression exists. At this site, the moraine has been removed by erosion suggesting that a higher transgressive episode of the lake has favored water routing from the Lago Negro to the General Carrera Lake. This reinforces the conceptual model proposed by Hein et al. (2010), Bell (2008) and Turner (2005) who have proposed that the PC Lake out flowed toward the GCBA Lake through the Rio Baker valley as caused by ice-damming preventing any discharge towards the Pacific. The geomorphological analyses of the Lago Negro and Lago Bertrand outlet areas and their evolution (Fig. 13) allow disentangling their development through time. First, a thick fan-delta accumulated, which elevation allows ascribing the sediment accumulation to the T1 terrace event. The fan delta forset layers (Fig. 13 D) document that stream-discharge was flowing eastward from the Lago Negro and Lago Bertrand towards the General Carrera Lake. Subsequently a prominent ridge moraine developed unconformably overlying the fan-delta accumulations and the basement rock. The ice was flowing to the east. Because strandlines notch the moraines (Fig. 12 B and C, 13 C) we infer that a major transgression event occurred afterward, flooding the moraine ridge.

#### 4.7. Rio Bayo/Rio Tranquilo area

The short depression along the Rio Tranquilo (flowing to the GCBA Lake) connecting to the Rio Bayo (flowing to the Pacific Ocean) marks the Present northern boundary of the NPI. The divide between the two rivers is at 371 m elevation. The Rio Tranquilo exhibits the typical morphology of a deep narrow glacial valley. The terminal moraine of a major glacier flowing northward from the NPI is damming the valley floor of the Rio Bayo. Glasser et al. (2005) have proposed that this terminal moraine dated back to the Little Ice Age. Subsequently, Glasser et al. (2006) have documented that ice mass remained in the Rio Bayo outlet glacier until  $9.7 \pm 0.7$  ka. Whatever is the age of the major ice recession along the Rio

Bayo/Rio Tranquilo depression, we do note that no erosion associated to the subsequent water drainage exists at the divide between the GCBA Lake and the Pacific. It suggests that the valley has never been a significant spillway for the GCBA Lake.

## 5. Discussion

### 5.1. Ice retreat, water routing, and climate inferences

The Buenos Aires Lake area (Argentina) has recorded two morpho-climatic stages. The first stage, which extends from the LGM (19-27 ka) to the ACR (12.9-14.5 ka), exhibits six ice lobe re-advances or still-stands recorded by the Menucos and Fenix I to V moraine ridges. The ice lobe had an oscillatory development, the cold episodes being separated by warmer periods of retreating ice front. No evidence exists for major retreats, the ice lobe remaining located along the Andean foreland. We infer modest climate fluctuations at the millennium time scale till the ACR. Water routing was from a pro-glacial lake toward the Atlantic Ocean. During the second stage the Buenos Aires Lake became free of ice and evolved as a major pro glacial lake for the remaining General Carrera ice lobe. The water level of the pro-glacial lake was controlled by the elevation of the Perito Moreno outlet (392 m at Present). Because (1) the braided pattern areas (Fig. 8) show no evidence for subsequent lake flooding higher than  $415 \pm 5$  m, and (2) the Rio Deseado spillway exhibits a very low water flow associated with no active erosion, we assume a significant rainfall deficit in this rain shadow area at the origin of the ice retreat following the ACR. A drainage re-arrangement occurred during the transition from stage 1 to stage 2 through the capture of the Rio Fenix Grande by the Rio Fenix Chico. No Significant water drainage toward the Atlantic Ocean existed at that time. Since then the GCBA Lake became an endorheic basin.

Five different episodes (T0 to T4, Table 2) of terrace development have recorded the evolution of the shoreline area of the General Carrera Lake. Since, the terrace T1 is older than the moraines described by Douglass et al. (2005) at Fachinal (revised ages at  $10.9 \pm 1.3$  ka), the more elevated terraces —i.e. T2 to T4 terraces— should be older. The oldest minimum CRE age obtain for dropstones on terraces ( $18.8 \pm 3.9$  ka, sample 71, Terrace T4, Table 1) constrains the maximum age for terraces accumulation. Also the accumulation of terraces T2 to T4, which evolved in an ice-walled lake environment along the main ice lobe of the General Carrera glacier, has likely to occur during the ACR from 12.9 to 14.5 ka. We

therefore infer that the accumulation of the terraces T1 to T4 occurred between 12.9-14.5 and  $10.9 \pm 1.3$  ka. The T0 terrace likely began accumulating after the younger Inner moraine at Facinal —age at  $7.9 \pm 1.1$  ka— that is in agreement with the age (younger than 6.7 ka) proposed by Bell (2008).

The accumulation of the T1 terrace, which extends all along both sides of the General Carrera Lake (Fig. 14), documents a period of relatively stable lake level associated with massive ice retreat. The western outlet area of the General Carrera Lake indicates that the Rio Baker was flowing eastward and draining the CP Lake watershed during that period. Turner et al. (2005) have first proposed such a drainage scenario. Subsequently, Hein et al. (2010) assumed the drainage system being active for the time window 15-16.5 ka. We regard the youngest limit to be too old by about  $\sim 0.5$  ka as a minimum. This drainage organization indeed suggests that ice damming along the Rio Baker was prohibiting any discharge to the Pacific. Because no significant drainage toward the Atlantic also existed during the time period from 12.9-14.5 to  $10.9 \pm 1.3$  ka, we infer that the Terrace T1 accumulated in an endorheic environment controlled by a severe rainfall deficit.

At the Lago Negro and Lago Bertrand spillways (GCBA Lake western outlet), moraine ridges overly the T1 terrace (Fig. 12 and 13). At both sites, the moraines were subsequently flooded. Two major morpho-climatic events punctuated the evolution of the GCBA Lake area after the terrace T1 accumulation. It includes a glacial advance during a neoglacial activity followed by a major flooding event. The post terrace T1 glacial advance was first documented and dated at Fachinal where two short episodes of glacier advance occurred at  $10.9 \pm 1.3$  and  $7.9 \pm 1.1$  ka. These two cold events may correlate the YD and the 8.2 Cold Event. Whatever they are, they have likely recorded an increase in precipitation and/or a decrease in temperature resulting from a northward migration of the Westerlies.

Subsequently, a major flooding of the two Holocene moraines re-advances occurred as documented at the GCBA Lake outlet area. Also, at the Rio de Las Dunas area (Fig. 9 and 10) a pervasive strandline imprint documents this major transgression phase. Topsets and cliffs of the T1 to T4 terrace fan-deltas exhibit regularly spaced notches and strandlines (tempestites) extending from 527 m to the lake level (201 m) at Present. The regularly nested shoreline pattern punctuate by storms suggests a steady smooth lowering of the lake from 527 m to 201 m. As exemplified at point X (Fig. 9), cold/wet events such as the Little Ice Age occurred during lake lowering phases. The dry climate and the incision of the Bertrand Lake outlet are the main processes at the origin of the GCBA Lake regression that occurred after the last major re-advance of glaciers at  $7.9 \pm 1.1$  ka. This regression is documented by drop-stones

sampled at the 53 and 73 sites (Fig 12 C and Fig. 9, respectively, and Table 1). Indeed, (1) sample 53 yields a minimum CRE age at  $8.6 \pm 2.0$  ka, a mid point age close to the 8.2-ka Cold Event as is the second cold event identified at Fachinal —i.e. the Inner moraine described by Douglass et al., (2005), mid point age at 7.9 ka—, (2) sample 73 that yields a minimum CRE age at  $9.9 \pm 2.5$  ka has been collected overlying a tempestite ridge at 521 m elevation. Therefore, the emplacement of the dropstone (sample 73) has to occur during the major flooding event following the second cold event at  $7.9 \pm 1.1$  ka. Although ages of samples 53 and 73 are imprecise, they provide evidences for climate events —i.e. the 8.2-ka Cold Event and the subsequent flooding event— occurring during/or after the 8.2-ka Cold Event.

The General Carrera Lake has recorded five morpho-climatic episodes. During the first episode, T2 to T4 terraces accumulated in ice-walled lake environment, as a major ice tongue existed along the General Carrera Lake. During the second episode, the disintegration of the ice tongue allowed a general distribution of the T1 terrace along the General Carrera Lake. Subsequently, two major ice advance occurred at  $\sim 10.9 \pm 1.3$  ka and  $\sim 7.9 \pm 1.1$  ka during the third episode. The fourth episode matches a general flooding that has reached the elevation of the highest T4 terrace. Because no evidence exists for the Perito Moreno eastern outlet being active in association with ice damming preventing drainage to the Pacific, we infer that the flooding event resulted from a rainfall enhancement after  $7.9 \pm 1.1$  ka. The fifth episode began as the western outlet opened and allowed drainage to the Pacific with no major disruption till the Present. We consider that all five episodes controlling the evolution of the General Carrera Lake post-date the first stage identified at the Buenos Aires Lake. Although the age and extent of the ACR is latitudinal controlled and controversial, it is accepted as a valuable age control for the colonization of recently deglaciated terrains by forests of *Nothofagus* ca. 12.3 ago (Moreno et al., 2009) at Torres del Paine area ( $\sim 51^\circ\text{S}$ ).

## 5.2. Glacial rebound

In a low viscosity regime of  $1 \times 10^{18}$  Pa s for the asthenosphere associated with an elastic lithosphere thickness of 35 km, Ivins and James (2004, 1999) have predicted rates of crustal vertical motion similar to those presently occurring in Fennoscandia, and eastern Canada (Lambeck et al., 1998; Wu, 1997; Mitrovica and Forte, 1997; Mitrovica and Peltier, 1992). Estimating ice volume loss for the past 4-5 ka, they calculated crustal uplift rates of 5 to 12



mm.yr<sup>-1</sup> for the NPI and SPI. Based on Global Positioning System (GPS) measurements performed between 2003 and 2006, Dietrich et al. (2010) have documented a vertical crustal uplift rate of 39 mm.yr<sup>-1</sup> for the SPI. This uplift rate is an order of magnitude higher than previously anticipated. They infer a response to an accelerated glacier wasting since the termination of the Little Ice Age (LIA) consistent with an effective regional mantle viscosity of  $\sim 4.0\text{-}8.0 \times 10^{18}$  Pa s. This low viscosity would originate from the asthenospheric mantle flow associated with the Patagonia slab window at depth. In addition, Dietrich et al. (2010) have anticipated the ability of even lower viscosity than those reported from young and dynamic volcanic regions due to the massive influx of volatiles through the slab window (Gorring and Kay, 2001). Dietrich et al. (2010) have documented that the large GPS uplift rates are generated by an integral response to glacier losses since the termination of the LIA in the late 19<sup>th</sup> Century.

Our data together with those of Douglass et al. (2005) allow reconstructing the morpho-tectonic situation by the end of the major transgression occurring after the ice re-advance at  $7.9 \pm 1.1$  ka (Fig. 15). (1) East of the GCBA Lake, the elevation of the divide at Perito Moreno (392 m at Present) is not accurately documented. From simple models, Ivins and James (2004; 1999) have predicted 1 mm.yr<sup>-1</sup> of vertical motion at the divide. Depending on the accepted glacier fluctuations, they have inferred both uplift and subsidence occurring during the Late Holocene and Present based on a likely elevation of  $\sim 392 \pm 6$  m at  $7.9 \pm 1.1$  ka. From GPS measurements, Dietrich et al. (2010) have extrapolated an uplift rate resulting from the SPI mass loss of 0.4-0.8 mm.yr<sup>-1</sup> for the area located between Chile Chico and Perito Moreno (Fig. 7). No uplift value resulting from the NPI ice loss is proposed. Finally, we consider the Present elevation (392 m) of the divide as a conservative value for our rebound calculation along the GCBA Lake (see below). (2) South of the Rio de Las Dunas fan-delta (Fig. 9 and 10), we have documented that the General Carrera Lake was at 326 m above its present elevation (201 m). Whether no tectonic deformation is considered for the past  $7.9 \pm 1.1$  ka, a lake level higher than the outlet at Perito Moreno must be considered. Therefore, we must consider an uplift correction that is the difference between the most elevated shoreline at  $7.9 \pm 1.1$  ka (527 m) and the elevation at the Perito Moreno outlet (392 m or less). Based on the Perito Moreno outlet elevation at  $7.9 \pm 1.1$  ka ago, a minimum uplift of 135 m for the Rio de Las Dunas area has thus to be considered. (3) West of the GCBA Lake, at the Lago Bertrand outlet (Fig. 12), two main bodies of evidences have been considered. First, flooding of the  $10.9 \pm 1.3$  to  $7.9 \pm 1.1$  ka moraines occurred during a major transgression episode that reached 527 m at the Rio de Las Dunas, the lake elevation at both sites —i.e. the Rio de Las

Dunas and the Lago Bertrand outlet— being controlled by ice damming along the Rio Baker. Second, the incision at the Lago Bertrand outlet has completely removed the moraine ridge accumulated at  $10.9 \pm 1.3$  to  $7.9 \pm 1.1$  ka. Because the unconformity of the underlying T1 terrace with the basement rock is not clearly identified, no confident incision measurement is possible at this site. Considering that the GCBA Lake is the local base level for its tributaries, an incision at the Lago Bertrand outlet from incision measurement at tributaries was calculated. The Rio Müller (Fig. 11) and Rio El Salto (Fig. 3 D), two of the lake tributaries, have recorded incisions of 94 and 102 m, respectively. We therefore infer that a down cutting of  $\sim 98$  m (average of incision along tributaries) has occurred at the GCBA Lake outlet documenting an incision rate of 10.9 to 14.4 mm.yr<sup>-1</sup> for the past  $7.9 \pm 1.1$  ka.

The  $\sim 326$  m amplitude of lake level variation (Fig. 15) should be split into an incision signal of  $\sim 98$  m and a remaining rebound signal of 228 m (maximum value). A rebound signal ranging from 228 to 135 m highlighted in an area located at Rio de Las Dunas yields to an uplift rate between 15 and 33.5 mm.yr<sup>-1</sup> for the past  $7.9 \pm 1.1$  ka. Assuming a permanent rainfall deficit in this rain shadow area, the largest uplift rate is the most likely. If accepted, this assumption implies that the average uplift rate at the Rio de Las Dunas area calculated over the past  $7.9 \pm 1.1$  ka is in the same order than that derived from the GPS measurements (39 mm.yr<sup>-1</sup>) performed between 2003 and 2006 along a SPI transect (Dietrich et al., 2010). Considering the slab window-induced low viscosity at depth and the elastic lithosphere thickness as local invariants, we infer that the high uplift rates calculated over the past  $7.9 \pm 1.1$  ka originated mainly from ice loss as it was proposed for the time period following the termination of the LIA. We suggest that (1) massive ice loss occurred not only during the last century but dated back to several ka in the past, and (2) the ice re-advances at  $7.9 \pm 1.1$  ka is likely more significant than anticipated.

## 6. Conclusions

- Relative chronology of morpho-climatic records together with 18 cosmogenic <sup>10</sup>Be ages and available data allow us constraining the timing of the Patagonian ice-sheet fluctuations since the LGM.
- The estimated thickness of ice along the GCBA lobe at the longitude of Chile Chico (Argentina-Chile border) is  $\sim 1.5$  to 1.7 km during the LGM. The estimated ELA at

that time is  $\sim 1100$  m (no rebound correction), an elevation similar to that proposed for the Chilean Lakes region during the LGM.

- The Buenos Aires Lake area (Argentina) has recorded two morpho-climatic stages. The first one extends from the LGM (19-27 ka) to the ACR (12.9-14.5 ka). The ice lobe front has been oscillating at the millennial scale remaining located along the Andean foreland. During the second stage the Buenos Aires Lake became free of ice. A significant rainfall deficit in this rain shadow area was coeval with the ice retreat following the ACR, the GCBA Lake becoming an endorheic basin.
- The General Carrera Lake evolved through five morpho-climatic episodes, all likely younger than 12.9-14.5 ka. During the first and the second episode the lake evolved as an endorheic basin from  $10.9 \pm 1.3$  to 12.9 ka. Two cold events associated with glacier re-advance occurred at  $7.9 \pm 1.1$  and  $10.9 \pm 1.3$  ka during the third episode. These cold events may relate to the 8.2-ka Cold Event and the YD, respectively. A major flooding younger than  $7.9 \pm 1.1$  ka resulted from a rainfall enhancement occurring during the fourth episode. The fifth episode began as the western outlet of the GCBA Lake opened allowing drainage to the Pacific with no major disruption till the Present
- We highlight a rebound signal ranging from 135 m to 228 m in an area located at Rio de Las Dunas (General Carrera Lake). The uplift rate (glacial rebound) ranges between 15 and 33.5 mm.yr<sup>-1</sup> for the past  $7.9 \pm 1.1$  ka.
- The average uplift rate of the Rio de Las Dunas area calculated over the past  $7.9 \pm 1.1$  ka is in the same order than the GPS measurements (39 mm.yr<sup>-1</sup>) performed between 2003 and 2006 along a SPI transect (Dietrick et al., 2010). We infer that the high uplift rates calculated over the past  $7.9 \pm 1.1$  ka mainly resulted from ice loss.
- We suggest that (1) massive ice loss occurred not only during the last century but dated back to several ka, and (2) the ice re-advance at  $7.9 \pm 1.1$  ka is more significant than previously thought.
- A down cutting of  $\sim 98$  m has occurred at the western GCBA Lake outlet documenting an elevated incision rate of 10.9 to 14.4 mm.yr<sup>-1</sup> during the past 6.8-9 ka.

## Acknowledgments

The ECOS-CONICYT program has funded this work through the project C96U01. We are grateful to the Université Pierre et Marie Curie (UPMC, Paris 6) and the Centre National de la Recherche Scientifique (CNRS, France). The Institut National des Sciences de l'Univers

(INSU) has provided support at the initiation of the project. SERNAGEOMIN (Villarrica) and the Universidad de Concepcion (GEA) have provided logistical support for fieldwork. We thank the Dr David B. Rowley and an anonymous reviewer for their helpful reviews that greatly improved the original manuscript.

## References

Ackert, Jr.R.P.; Singer, B.S.; Guillou, H.; Kaplan, M.R.; and Kurz, M.D. 2003. Long-term cosmogenic  $^3\text{He}$  production rates from  $^{40}\text{Ar}/^{39}\text{Ar}$  and K-Ar dated Patagonian lava flows at 47°S. *Earth and Planetary Science Letters* 210, 119-136.

Alley, R.B. 2000. The Younger Dryas cold interval as viewed from central Greenland. *Quaternary Science Reviews* 19, 213-226.

Alley, R.B.; Mayewski, P.A.; Sowers, T.; Stuiver, M.; Taylor, K.C.; and Clark, P.U. 1997. Holocene climatic instability: a prominent, widespread event 8200 yr ago. *Geology* 25, 483-486. doi: 10.1130/0091-7613(1997)025<0483:HCIAPW>2.3.CO;2.

Aniya, M.; Sato, H.; Naruse, R.; Skvarca, P.; Casassa, G. 1996. The use of satellite and airborne imagery to inventory outlet glaciers of the Southern Patagonia Icefield, South America. *Photogrammetric Engineering & Remote Sensing* 62, 1361-1369.

Aniya, M. 1988. Glacier inventory for the Northern Patagonia Icefield, Chile, and variations 1944/45 to 1985/86. *Arctic, Antarctic and Alpine Research* 20, 179-187.

Bakke J.; Nesje, A. 2011. The equilibrium line altitude (ELA): *Encyclopedia of snow, ice and glaciers*. Springer, 268-277.

Bell, C.M. 2008. Punctuated drainage of an ice-dammed Quaternary lake in southern South America. *Geografiska Annaler* 90, 1-17.

Behrmann, J.H.; Lewis, S.D.; and ODP Leg 141 Scientific Party 1992. Geology and tectonics of the Chile triple junction. *Eos (Transactions, American Geophysical Union)* 73, 404-405, 410.

- Blard, P-H.; Braucher, R.; Lavé, J.; Bourlès, D.L. 2013. Cosmogenic  $^{10}\text{Be}$  Production Rate Calibrated Against  $^3\text{He}$  in the High Tropical Andes (3800-4900 m, 20-22°S). *Earth and Planetary Science Letters* 382, 140-149.
- Boex, J.; Fogwill, C.; Harrison, S.; Glasser, N.F.; Hein, A.; Schnabel, C.; Xu, S. 2013. Rapid thinning of the late Pleistocene Patagonian Ice Sheet followed migration of the Southern Westerlies. *Nature Scientific Reports* 3, 2118, DOI:10.1038/srep02118.
- Bourgois, J.; Michaud, F. 2002. Comparison between the Chile and Mexico triple junction areas substantiates slab window development beneath northwestern Mexico during the past 12-10 Myr. *Earth and Planetary Science Letters* 201, 35-44.
- Bourgois, J.; Guivel, C.; Lagabrielle, Y.; Calmus, T.; Boulègue, J.; and Daux, V. 2000. Glacial-interglacial trench supply variation, spreading-ridge subduction, and feedback controls on the Andean margin development at the Chile triple junction area (45-48°S). *Journal of Geophysical Research* 105, 8355-8386.
- Bourlès, D. L. 1988. Etude de la géochimie de l'isotope cosmogénique  $^{10}\text{Be}$  et de son isotope stable en milieu océanique. Application à la datation de sédiments marins. PhD, Paris Sud Centre d'Orsay University, Orsay, France.
- Braucher, R.; Merchel, S.; Borgomano, J.; Bourlès, D.L. 2011. Production of cosmogenic radionuclides at great depth: a multi element approach. *Earth and Planetary Science Letters* 309(1-2), 1-9.
- Breitsprecher, K.; and Thorkelson, D.J. 2009. Neogene kinematic history of Nazca-Antarctic-Phoenix slab windows beneath Patagonia and Antarctic Peninsula. *Tectonophysics* 464, 10-20.
- Brown, E. T.; Brook, E.J.; Raisbeck, G.M.; Yiou, F.; and Kurz, M.D. 1992. Effective attenuation lengths of cosmic producing  $^{10}\text{Be}$  and  $^{26}\text{Al}$  in quartz, implications for exposure age dating. *Geophysical Research Letters* 19, 369– 372.

- Brown, E.T.; Edmond, J.M.; Raisbeck, G.M.; Yiou, F.; Kurz, M.D.; Brook, E.J. 1991. Examination of surface exposure ages of Antarctic moraines using in situ produced  $^{10}\text{Be}$  and  $^{26}\text{Al}$ . *Geochimica et Cosmochimica Acta* 55, 2269–2283.
- Caldenius, C.G. 1932. Las glaciaciones Cuaternarias en la Patagonia and Tierra de Fuego. *Geografiska Annaler* 14, 1-164.
- Cande, S.C.; and Leslie R.B. 1986. Late Cenozoic tectonics of the southern Chile trench. *Journal of Geophysical Research* 92, 495-520.
- Casassa, G. 1987. Ice thickness deduced from gravity anomalies on Soler glacier, Neff glacier and the northern Patagonia Icefield. *Bulletin of Glacier Research* 4, 43-57.
- Chmeleff, J.; von Blanckenburg, F.; Kossert, K.; and Jakob, J. 2010. Determination of the  $^{10}\text{Be}$  half-life by multicollector ICP-MS and liquid scintillation counting. *Nuclear Instruments and Methods in Physics Research B* 268, 192–199.
- Clapperton, C.M. 1997. Fluctuations of local glaciers 30-8 ka B.P.: overview. *Quaternary International* 38/39, 3-6.
- DeLong, S.E.; Fox, P.J.; MacDowell, F.W. 1978. Subduction of the Kula Ridge at the Aleutian Trench: *Geological Society of America Bulletin* 89, 83-95.
- Dickinson, W.R.; Snyder, W.S. 1979. Geometry of subducted slabs related to San Andreas transform. *Journal of Geology* 87, 609-627.
- Dietrich, R.; Ivins, E.R.; Casassa, G.; Lange, H.; Wendt, J.; Fritsche, M. 2010. Rapid crustal uplift in Patagonia due to enhanced ice loss. *Earth and Planetary Science Letters* 289, 22-29.
- Douglass, D.C.; Singer, B.S.; Kaplan, M.R.; Mickelson, D.M.; Caffee, M.W. 2006. Cosmogenic nuclide surface exposure dating of boulders on last-glacial and late-glacial moraines, lago Buenos Aires, Argentina: interpretative strategies and paleoclimate implications. *Quaternary Geochronology* 1, 43-58.

- Douglass, D.C.; Singer, B.S.; Kaplan, M.R.; Ackert, R.P.; Mickelson, D.M.; Caffee, M.W. 2005. Evidence of early Holocene glacial advances in southern South America from cosmogenic surface-exposure dating. *Geology* 33, 237-240.
- Fleming, K.; Johnston, P.; Zwart, D.; Yokoyama, Y.; Lambeck, K.; Chappell, J. 1998. Refining the eustatic sea-level curve since the Last Glacial Maximum using far- and intermediate-field sites. *Earth and Planetary Science Letters* 163, 327-342.
- Garreaud, R.; Lopez, P.; Minvielle, M.; and Rojas, M. 2013. Large-scale control on the Patagonia climate. *Journal of Climate, American Meteorological Society* 26, 215-230, DOI: 10.1175/JCLI-D-12-00001.1.
- Glasser, N.F., Harrison, S.; Schnabel, C.; Fabel, D.; Jansson K.N. 2012. Younger Dryas and early Holocene age glacier advances in Patagonia. *Quaternary Science Reviews* 58, 7-17.
- Glasser, N.F.; Harrison, S.; Ivy-Ochs, S.; Duller, G. A. T.; Kubik, P. W. 2006. Evidence from the Rio Bayo valley on the extent of the North Patagonian Icefield during the Late Pleistocene-Holocene transition. *Quaternary Research* 65, 70-77.
- Glasser, N.F.; Jansson, K.N.; Harrison, S.; Rivera, A. 2005. Geomorphological evidence for variations of the North Patagonian Icefield during the Holocene. *Geomorphology* 71, 263-277.
- Gorring, M.; Singer, B.; Gowers, J.; and Kay, S. 2003. Plio-Pleistocene basalts from the Meseta del Lago Buenos Aires, Argentina: evidence for asthenosphere-lithosphere interactions during slab window magmatism. *Chemical Geology* 193, 215-235.
- Gorring, M.; and Kay, S. 2001. Mantle processes and sources of Neogene slab window magmas from southern Patagonia, Argentina. *Journal of Petrology* 42, 1067–1094. doi:10.1093/petrology/42.6.1067.

- Gorring, M.L.; Kay, S.M.; Zeitler, P.K.; Ramos, V.A.; Rubiolo, D.; Fernandez, M.I.; and Panza, J.L. 1997. Neogene Patagonian plateau lavas: continental magmas associated with ridge collision at the Chile triple junction. *Tectonics* 16, 1-17.
- Guivel, C.; Morata, D.; Pelleter, E.; Espinoza, F.; Maury, R.; Lagabriele, Y.; Polvé, M.; Bellon, H.; Cotton, J.; Benoit, M.; Suarez, M.; de la Cruz, R. 2006. Miocene to Late Quaternary Patagonian basalts (46-47° S): geochronometric and geochemical evidence for slab tearing due to active spreading ridge subduction. *Journal of Volcanology and Geothermal Research* 149, 346-370.
- Hein, A.S.; Hulton, N.R.J.; Dunai, T.J.; Sugden, D.E.; Kaplan, M.R.; Xu, S. 2010. The chronology of the Last Glacial Maximum and deglacial events in central Argentine Patagonia. *Quaternary Science Reviews* 29, 1212-1227. doi:10.1016/j.quascirev.2010.01.020
- Hein, A.S.; Hulton, N.R.J.; Dunai, T.J.; Schnabel, C.; Kaplan, M.R.; Naylor, M.; Xu, S. 2009. Middle Pleistocene glaciation in Patagonia dated by cosmogenic-nuclide measurements on outwash gravels. *Earth and Planetary Science Letters* 286, 184-197, Doi:10.1016/j.epsl.2009.06.026
- Hoffman, J.A.J. 1975. *Atlas Climatico de America del Sur*. WMO, Unesco, Geneva.
- Hulton, N.R.J.; Purves, R.S.; McCulloch, R.D.; Sugden, D. E.; Bentley, M.J. 2002. The Last Glacial Maximum and deglaciation in southern South America. *Quaternary Science Reviews* 21, 233-241.
- Hulton, N.R.J.; and Sugden, D.E. 1997. Dynamics of mountain ice caps during glacial cycles: the case of Patagonia. *Annals of Glaciology* 24, 81-89.
- Hulton, N.D.; Sugden, D.; Payne, A.; and Clapperton, C. 1994. Glacier modeling and climate of Patagonia during the last glacial maximum. *Quaternary Research* 42, 1-19.



- Ivins, E.R.; and James, T.S. 2004. Bedrock response to Llanquihue Holocene and present-day glaciation in southernmost South America. *Geophysical Research Letters* 31, L24613, doi:10.1029/2004GL021500.
- Ivins, E.R.; and James, T.S. 1999. Simple models for late Holocene and Present-day Patagonian glacier fluctuations and predictions of a geodetically detectable isostatic response. *Geophysical Journal International* 138, 601-624.
- Jomelli, V.; Favier, V.; Vuille, M.; Braucher, R.; Martin, L.; Blard, H.; Colose, C.; Brunstein, D.; He, F.; Khodri, M.; Bourles, D.; Leanni, L.; Rinterknecht, V.; Grancher, D.; Francou, B.; Ceballos, J.L.; Fonseca, H.; Liu, Z.; and Otto-Bliesner, B.L. 2014. A major advance of tropical Andean glaciers during the Antarctic cold reversal. *Letter to Nature*, doi:10.1038/nature13546.
- Kaplan, M.R.; Strelin, J.A.; Schaefer, J.M.; Denton, G.H.; Finkel, R.C.; Schwartz, R.; Putnam, A.E.; Vandergoes, M.J.; Goehring, B.M.; Travis, S.G. 2011. In-situ cosmogenic  $^{10}\text{Be}$  production rate at Lago Argentino, Patagonia: Implications for late-glacial climate chronology. *Earth and Planetary Science Letters* 309, 21–32.
- Kaplan, M.R.; Ackert, R.P.; Singer, B.S.; Douglass, D.C.; and Kurz, M.D. 2004. Cosmogenic nuclide chronology of millennial-scale glacial advances during O-isotope stage 2 in Patagonia. *Geological Society of America Bulletin* 116, 308-321, doi: 10.1130/B25178.1.
- Kelly, M.A.; Lowell, T.V.; Applegate, P.J.; Phillips, F.M.; Schaefer, J.M.; Smith, C.A.; Kim, H.; Leonard, K.C.; and Hudson A.M. 2014. A locally calibrated, late glacial  $^{10}\text{Be}$  production rate from a low-latitude, high-altitude site in the Peruvian Andes. *Quaternary Geochronology*, <http://dx.doi.org/10.1016/j.quageo.2013.10.007>
- Klemann, V.; Ivins, E.R.; Martinec, Z.; and Wolf, D. 2007. Models of active glacial isostasy roofing warm subduction: case of the South Patagonia Icefield. *Journal of Geophysical Research* 112, B09405, doi:10.1029/2006JB004818.

- Korschinek, G.; Bergmaier, A.; Faestermann, T.; Gerstmann, U.C.; Knie, K.; Rugel, G.; Wallner, A.; Dillmann, I.; Dollinger, G.; Lierse von Gostomski, Ch.; Kossert, K.; Maitia, M.; Poutivtsev, M.; and Remmert, A. 2010. A new value for the half-life of  $^{10}\text{Be}$  by Heavy-Ion Elastic Recoil Detection and liquid scintillation counting. *Nuclear Instruments and Methods in Physics Research B*. 268, 187–191.
- Lal, D. 1991a. The present scope of the field of terrestrial cosmogenic nuclides. *Science* 6, 744-751.
- Lal, D. 1991b. Cosmic ray labeling of erosion surfaces: In situ nuclide production rates and erosion models. *Earth and Planetary Science Letters* 104, 424–439,
- Lambeck, K., Smither, C., and Johnston, P., 1998. Sea-level change, glacial rebound and mantle viscosity for northern Europe. *Geophysical Journal International* 134, 102-144.
- Leslie, R.B. 1986. Cenozoic tectonics of southern Chile triple junction migration, ridge subduction, and forearc evolution. PhD thesis, 276 pp., Columbia University, New York.
- Lowell, T.V.; Heusser, C.J.; Andersen, B.G.; Moreno, P.I.; Hauser, A.; Heusser, L.E.; Schlüchter, C.; Marchant, D.R.; and Denton, G.H. 1995. Interhemispheric correlation of Late Pleistocene glacial events. *Science* 269, 1541-1549.
- Marden, C.J.; and Clapperton, C.M. 1995. Fluctuations of the South Patagonia Icefields during the last glaciation and the Holocene. *Journal of Quaternary Science* 10, 197-210.
- Markgraf, V.; Dodson, J.R.; Kershaw, A.P.; McGlone, S.; and Nicholls, N. 1992. Evolution of Late Pleistocene and Holocene climates in the circum-South Pacific land areas. *Climate Dynamics* 6, 193-211.
- Mercer, J.H. 1982. Holocene glacier variations in Southern South America. *Striae* 18, 35-40.
- Merchel, S.; and Herpers, U. 1999. An update on radiochemical separation techniques for the determination of long-lived radionuclides via Accelerator Mass Spectrometry. *Radiochimica Acta* 84, 215–219.

- Miller, A. 1976. The climate of Chile, in World Survey of Climatology, vol. 12. Climates of Central Chile and South America, edited by W. Schwerdtfeger, 113-145, Elsevier, Amsterdam-Oxford-New York.
- Mitrovica, J.X.; and Forte, A. 1997. Radial profile of mantle viscosity: results from the joint inversion of convection and post-glacial rebound observables. *Journal of Geophysical Research* 102, 2751-2769.
- Mitrovica, J.X.; and Peltier, W.R. 1992. Constraints on mantle viscosity from relative sea level variations in Hudson bay. *Geophysical Research Letters* 19, 1185-1188.
- Moreno, P.L.; Kaplan, M.R.; François, J.P.; Villa-Martinez, R.; Moy, C.M.; Stern, C.R.; Kubik, P.W. 2009. Renewed glacial activity during the Antarctic Cold Reversal and persistence of cold conditions until 11.5 ka in southwestern Patagonia. *Geology* 37, 375-378. doi: 10.1130/G25399A.
- Murdie, R.E.; Pugh, D.T.; Styles, P. 1999. A lightweight, portable, digital probe for measuring the thermal gradient in shallow water sediments, with examples from Patagonia. *Geo-Marine Letters* 18, 315-320.
- Orihashi, Y.; Anma, R.; Motoki, A.; Haller M.J.; Hirata, D.; Iwano, H.; Sumino, H.; Ramos, A. 2013. Evolution history of the crust underlying Cerro Pampa, Argentine Patagonia: constraint from LA-ICPMS U-Pb ages for exotic zircons in the Mid-Miocene adakite. *Geochemical Journal* 47, 235-247.
- Peck, V.L.; Hall, I.R.; Zahn, R.; Grousset, F.; Hemming, S.R.; Scourse, J.D. 2007. The relationship of Heinrich events and their European precursors over the past 60 ka BP: a multi-proxy ice-rafted debris provenance study in the northeast Atlantic. *Quaternary Science Reviews* 26, 862-875. doi:10.1016/j.quascirev.2006.12.002.
- Porter, S.C. 1981. Pleistocene glaciation in the southern Lake District of Chile. *Quaternary Research* 16, 263-292.

- Raisbeck, G. M.; Yiou, F.; Bourles, D. L.; Brown, E.T.; Deboffle, D.; Jouhannau, P.; Lestringuez, J.; and Zhou, Z.Q. 1994. The AMS facility at Gif-sur-Yvette: Progress, perturbations and projects. *Nuclear Instruments and Methods in Physics Research B* 92, 43-46.
- Raisbeck, G. M.; Yiou, F.; Bourlès, D.L.; Lestringuez, J.; and Deboffle, D. 1987. Measurements of  $^{10}\text{Be}$  and  $^{26}\text{Al}$  with a Tandetron AMS facility. *Nuclear Instruments and Methods in Physics Research B* 29, 22-26.
- Rivera, A.; Benham, T.; Casassa, G.; Bamber, J.; Dowdeswell, J.A. 2007. Ice elevation and areal changes of glaciers from the northern Patagonia Icefield, Chile. *Global and Planetary Change* 59, 126-137.
- Russo, R.M.; VanDecar, J.C.; Comte, D.; Mocanu, V.I.; Gallego, A.; and Murdie, R.E. 2012. Subduction of the Chile ridge: upper mantle structure and flow. *GSA Today* (20) 9, 4-10. doi: 10.1130/GSATG61A.1.
- SERNAGEOMIN 2002. Carta Geologica de Chile, N°75, Escala: 1,000,000, Hoja 3, Servicio Nacional de Geología y Minería, Subdirección Nacional de Geología, Chile.
- Singer, B.S.; Ackert, R.P.; and Guillou, H. 2004.  $^{40}\text{Ar}/^{39}\text{Ar}$  and K-Ar chronology of Pleistocene glaciations in Patagonia. *Geological Society of America Bulletin* 116, 434-450, doi: 10.1130/B25177.1
- Singer, B.; Hildreth, W.; Vincze, Y. 2000.  $^{40}\text{Ar}/^{39}\text{Ar}$  evidence for early deglaciation of the central Chilean Andes. *Geophysical Research Letters* 27, 1663-1666.
- Stone, J.O. 2000. Air pressure and cosmogenic isotope production. *Journal of Geophysical Research* (105) 23, 753-759.
- Sugden, D.E.; Hulton, N.R.J.; Purves, R.S. 2002. Modelling the inception of the Patagonian icesheet. *Quaternary International* 95-96, 55-64.

Turner, K.J.; Fogwill, C.J.; McCulloch, R.D.; Sugden, D.E. 2005. Deglaciation of the eastern flank of the North Patagonian Icefield and associated continental-scale lake diversions. *Geogr. Ann.*, 87A(2), 363-374.

Wenzens, G. 2005. Glacier advances east of the Southern Andes between the Last Glacial Maximum and 5,000 BP compared with lake terraces of the endorrheic Lago Cardiel (49 degrees S, Patagonia, Argentina). *Zeitschrift Fr Geomorphologie* 49, 433-454.

Wenzens, G. 1999. Fluctuations of outlet and valley glaciers in the Southern Andes (Argentina) during the past 13,000 years. *Quaternary Research* 51, 238-247.

Wu, P. 1997. Effect of viscosity structure on fault potential and stress orientations in eastern Canada. *Geophysical Journal International* 130, 365-382.

# Figure captions and tables

**Table 1.** Minimum Cosmic Ray (CRE) ages calculated from in situ produced <sup>10</sup>Be concentrations within morphological markers. Location of samples (Fig. 2).

**Table 2.** Elevation and age for terraces along the General Carrera Lake between 72°50' and 70°57' W. The data are graphically used at Fig. 14. A-Avellano; Al-Puerto Alarcon; DE-Dunas E; DW-Dunas W; EP-El Porvenir; FS-Fachinal; HW-Las Horquetas W; IB-Puerto Ibañez; LB-Lago Bertrand; LN—Lago Negro; Mu-Murta; Ma-Maitenes; PB-Punta Baja; PM-Perito Moreno; S-Sanchez. fan-fan delta sediment; N-north shore; S-south shore; stra-strandline; T0 to T4-Terraces 0 to 4; green-sample number; red-sample age (ka); black-strandline elevation (m); **bold**-terrace elevation (max); *italic*-terrace elevation (min). Note that age at the third column from the left is from Lago Negro (LN). Location of samples at Fig. 2.

**Figure 1.** Location of the studied area (glacial extent during the LGM from Hulton et al., 1994; Caldenius, 1932). Grey is icefield including the North (NPI) and the South (SPI) Patagonian icefields at Present time. Khaki and white arrows show the locus of Westerlies and maximum moisture during the LGM (i.e. Oxygen Isotope Stage 2) and at Present, respectively. Subduction of the active spreading center along the Chile ridge occurs at the Chile triple junction (Bourgois et al., 2000) inducing the Patagonia slab window to develop at depth

beneath the South America plate. The red dash line shows the Patagonia slab window development at depth (Russo et al., 2012; Breitsprecher and Thorkelson, 2009; Bourgois and Michaud, 2002). Note that the General Carrera-Buenos Aires Lake area is located along the northern boundary of the Patagonia slab window at depth. CTJ–Chile Triple Junction; GCBA–General Carrera-Buenos Aires Lake; NPI–North Patagonian icefield; PSW–Patagonia slab window; SPI–South Patagonian icefield. Location of Fig. 2 is shown.

**Figure 2.** Location of sampling sites (ages, Table 1) along the GCBA Lake area. Note that the GCBA Lake outflows to the Pacific Ocean through the Rio Baker at Present. Two different outlet heads have been potentially active during the past 27 ka: the Rio Bayo to the Pacific, and the Rio Deseado (see Fig. 7 for location) to the Atlantic. Note that a short segment of the Rio Baker valley connects the Pueyrredon-Cochrane Lake (152 m at Present) to the GCBA Lake (201 m at Present. Location of Fig. 7, 9, 11, 12, and 13 is shown.

**Figure 3.** Terraces and strandlines along the GCBA Lake. A, B northern rim, from east to west: (A) T0 to T2 terraces at Pto Ingeniero Ibañez (location Fig. 2 and 7); (B) T0 to T2 terraces at Rio Avellano, (location Fig. 2). C to F southern rim from east to west: (C) Strandline at 226-230 m, east of Los Antiguos (Location, Fig. 2 and 7), Buenos Aires Lake (Argentina); (D) T1 terrace at Rio El Salto (46°34'06"S-72°05'50"W, location Fig. 2), note the typical Gilbert signature of the T1 terrace and the ~102 m deep incision of the basement rock (see text for more details); (E) T1 and T2 terraces at Rio de Las Dunas (location Fig. 2 and 9); (F) T1 and T2 terraces and associated strandlines in an area located 4-5 km east of Pto Guadal (location Fig. 2).

**Figure 4.** Fluctuating lake level regression and strandline records. (A) Alluvial fan delta at the Rio El Cañal (location Fig.2) outflow. A sequence of tempestite barriers characterizes the frontal part of the delta. Behind the coarse pebble barrier topset fine layers is accumulating. (B) Bay located few km east of Pto Guadal (location Fig. 2) exhibiting three successive tempestite barriers. Difference in elevation from right to left is about 3.5 m evidencing that GCBA Lake is regressing at Present. (C) Major sequence of strandline regression at Rio Las Dunas outflow area (Location Fig. 2 and 9). Note the pervasive signature of regressive strandline along the T1 terrace cliff (point Y3, see Fig. 10 and text for more details). Lake regression is continuous between 320 m and 201 m. Tempests during short phases of stable water level left a strandline imprint (point Y1, see Fig. 10 and text for more details). (D) A sequence of strandlines (point

Y6, see Fig. 10) similar to that at points Y1 and Y3 was identified at more than 500 m elevation indicating that processes of lake regression worked during a long regressive phase leaving a pervasive imprint at various elevations between 527 m and 201 m across the major terraces.

**Figure 5.** Moraine boulder and drop-stones. (A) Sample 15 (location Fig. 2 and 7), moraine boulder at the crest of a frontal moraine damming the Rio Fenix Chico river. This moraine, younger than the Menucos till, has recorded the last ice re-advance to the east (see text for more details). (B) Sample 31 (location Fig. 2 and 9), drop-stone atop the T3 terrace, note figure on the right for scale. (C) Sample 39 (Fig. 2 and 13A for location), drop stone on lake sediment accumulation. (D) Sample 57 (location Fig. 2 and 9), at this site tens of big drop stones exist. See text for more details.

**Figure 6.** Chronology for moraine boulders, drop stones on terraces, and glacial polish surface for collected samples. Horizontal bars indicate  $\pm 1\sigma$  uncertainties for  $^{10}\text{Be}$  CRE ages (Table 1). The lower panel shows ages for the moraine samples (blue numbers: western Bertrand outlet; brown numbers: eastern Perito Moreno outlet). Also shown are ages for six of the youngest moraines east of General Carrera-Buenos Aires Lake, which includes the Menucos (M) and the Fenix (FI to FV) moraines from the youngest to the oldest –i.e. from west to east– (thick dash line, ages from Kaplan et al., 2011).

The central panel shows ages for dropstones (black numbers) on terraces, sample 25 is from a glacial polish. Brown error bars show the recalculated ages for moraines described by Douglass et al. (2005) at Fachinal (location Fig. 2).

The upper panel shows the GISP2 ice core temperature for the Northern Hemisphere (Alley, 2000). The cold event at 8.2 kyr (Alley et al., 1997) and the Heinrich events H1 and H2 (Peck et al., 2007) are also shown. Note that the end of the Antarctic Cold Reversal (at 12.9 ka, Jomelli et al., 2014; Kaplan et al., 2011) coincides roughly with the estimated age of a significant increase of the *Nothofagus* southern beech pollen at 12.3 ka (Moreno et al., 2009).

**Figure 7.** Moraines at the Perito Moreno outlet area. From west to east –i.e. from the youngest to the oldest– it includes (Douglass et al., 2006; Kaplan et al., 2004; Singer et al., 2004; Ackert et al., 2003): the Menucos and Fenix I-V moraines ( $17.3 \pm 0.6$  to  $25.7 \pm 0.9$  ka), the Moreno I and II moraines ( $\sim 109$ -244 ka), the Moreno III-Deseado-Telken moraines ( $\sim 244$ -1016 ka). Note that the Rio Fenix Grande branches the Rio Fenix Chico at Perito Moreno (392 m, elevation at the divide between Pacific and Atlantic) to feed the GCBA Lake. At Present, no connection

exists between the Rio Fenix Grande and the Rio Deseado. Bold number—location of samples 4, 15, 17, 23 and 69; thin line with barb—main strandlines; thick violet dash-line—dry valley network. Location of Fig. 8 is shown; map location (west of 71°W) on Fig. 2.

**Figure 8.** Two contrasting morphological signatures recording the evolution of the Buenos Aires Lake. Above  $\sim 415 \pm 5$  m (northeastward) the pervasive braided pattern of meander loops characterizes an evolving ice lobe margin. Below  $415 \pm 5$  m (southwestward), parallel regressive strandlines document that the lake was free of ice. Note that the passage from one situation to the other exhibits a very sharp morphological signature suggesting a sharp ice retreat.

**Figure 9.** (A) Terraces along the Rio Los Maitenes. Note that sediment accumulated along a valley cutting across the T1 terrace (location at point X) evidencing a transgressive event occurring between T0 and T1. Location on Fig. 9B. (B) Terraces along the Rio de Las Dunas and Rio Las Horquetas-Los Maitenes. Five fan-delta terraces developed along these rivers, from the youngest to the oldest it includes: T0 (201-238 m); T1 (302-347 m); T2 (432-468 m); T3 (472-495 m); T4 (499-528 m). Dash line—strandline; bold number—location of samples 31, 57, 59, 61, 71, 73. Location on Fig. 2. Location of Fig. 9A and 10 is shown. See text for more details.

**Figure 10.** Pervasive strandline imprint at the Rio de Las Dunas area. Topsets and cliffs of fan-delta structures –i.e. T0 to T4 terraces– exhibit regularly spaced –i.e. every 2 to 3-5 m in elevation– notches associated with tempest. This is obvious along the cliff of terrace T1 at point Y3 (see also Fig. 4 C). The strandline network at point Y3 exhibits downslope prolongation along the bay area at points Y2 and Y1 (see also Fig. 4 C) down to the shoreline at Present. The pervasive strandline network exists across T2, T3 and T4 terraces at areas at points Y4, Y5, and Y6. Figure 4 D shows the area at point Y6. Lake regression shows a pervasive imprint throughout elevations from 527 to 201 m, across the major terraces. Location at Fig. 9.

**Figure 11.** Terrace development at Rio Müller. (A) Map showing the T0, T1, and T2 terraces. (B) Looking to the north from point L located at Fig. 11A. (C) Looking to the south from point M located at Fig. 11A. (D) A 94 m deep incision developed after the T1 terrace accumulation. See text for more details. Location at Fig. 2.



**Figure 12.** (A) The western outlet area of the General Carrera Lake. At Present, the GCBA Lake streams to the Pacific through the Lago Bertrand and the Rio Baker spillways. The location of Fig. 12 B, 12 C and 13 is shown. (B) Location of samples 45 and 49. (C) The outflow zone to the Rio Baker exhibits two moraines, the Inner moraine ridge has dammed the Lago Plomo, the Outer moraine has previously obstructed the Rio Baker discharge toward the Pacific Ocean. Note that strandline notches the older moraine (Fig. 12 B and 12 C). Location of samples 51, 53, 55 is shown. See text for more details.

**Figure 13.** (A) The Lago Negro outlet area. (B) Cross-section located at Fig. 13 A. (C) The basement rock extending west of the moraine (see Fig 13 B) shows strandline notches higher than the moraine. (D) The fan-delta sediment underlying the moraine ridge exhibits forsets dipping to the NE that documents drainage toward the General Carrera Lake.

**Figure 14.** Geomorphic markers and ages along the GCBA Lake. Note that: (1) ultimate ice retreat at Buenos Aires Lake dates back to the ACR (12.9-14.5 ka); (2) T2 to T4 terraces along the General Carrera Lake show local development; (3) as opposed, T0 and T1 extend along the General Carrera Lake throughout; (4) T1 is older than  $10.9 \pm 1.3$  ka; (5) the elevation versus Longitude regression line (purple line) for T1 terraces shows an eastward tilt (discussion of this tectonic deformation will be developed in a coming paper); (6) a major transgression phase occurred at  $\sim 7.9 \pm 2$  ka. A–Avellano; Al–Puerto Alarcon; DE–Dunas E; DW–Dunas W; EP–El Porvenir; FS–Fachinal; HW–Las Horquetas W; IB–Puerto Ibañez; LB–Lago Bertrand; LN–Lago Negro; Mu–Murta; Ma–Maitenes; PB–Punta Baja; PM–Perito Moreno; S–Sanchez. T0 to T4–terraces.

**Figure 15.** Basic data (rounded values) for calculating glacial isostatic rebound since the last major cold event at  $7.9 \pm 1.1$  ka. (A) Lago Bertrand outlet to the Pacific, (B) central area of the GCBA Lake —i.e. outlet of the Rio de Las Dunas area—, (C) Perito Moreno outlet at the divide between Pacific and Atlantic. Red dash line shows the lake level at  $7.9 \pm 1.1$  ka. Blue dash line, range elevation for ice damming at  $7.9 \pm 1.1$  ka. See text for more details.

Figure  
[Click here to download Figure: FIG 1 ICE CAP LOC.eps](#)

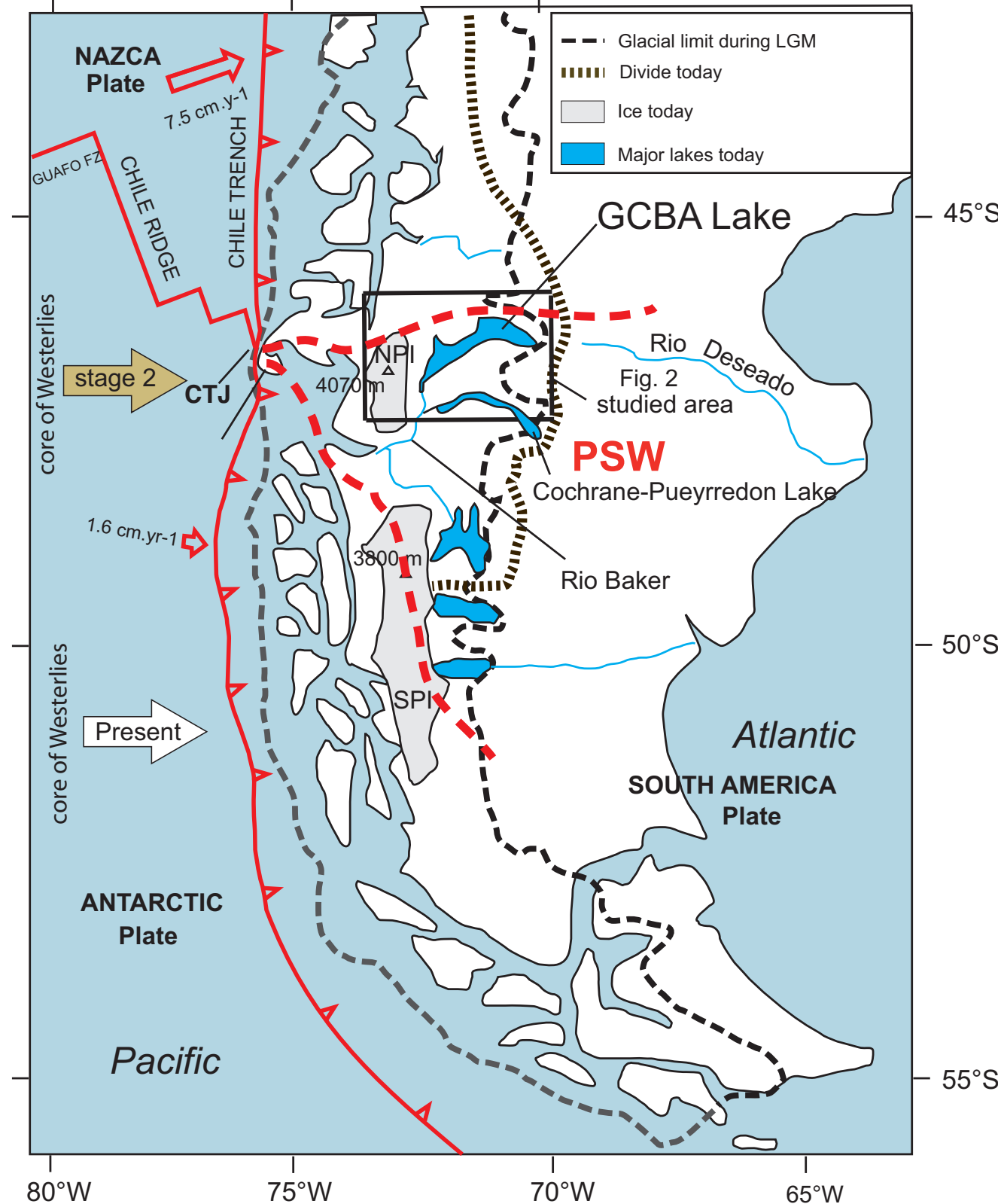
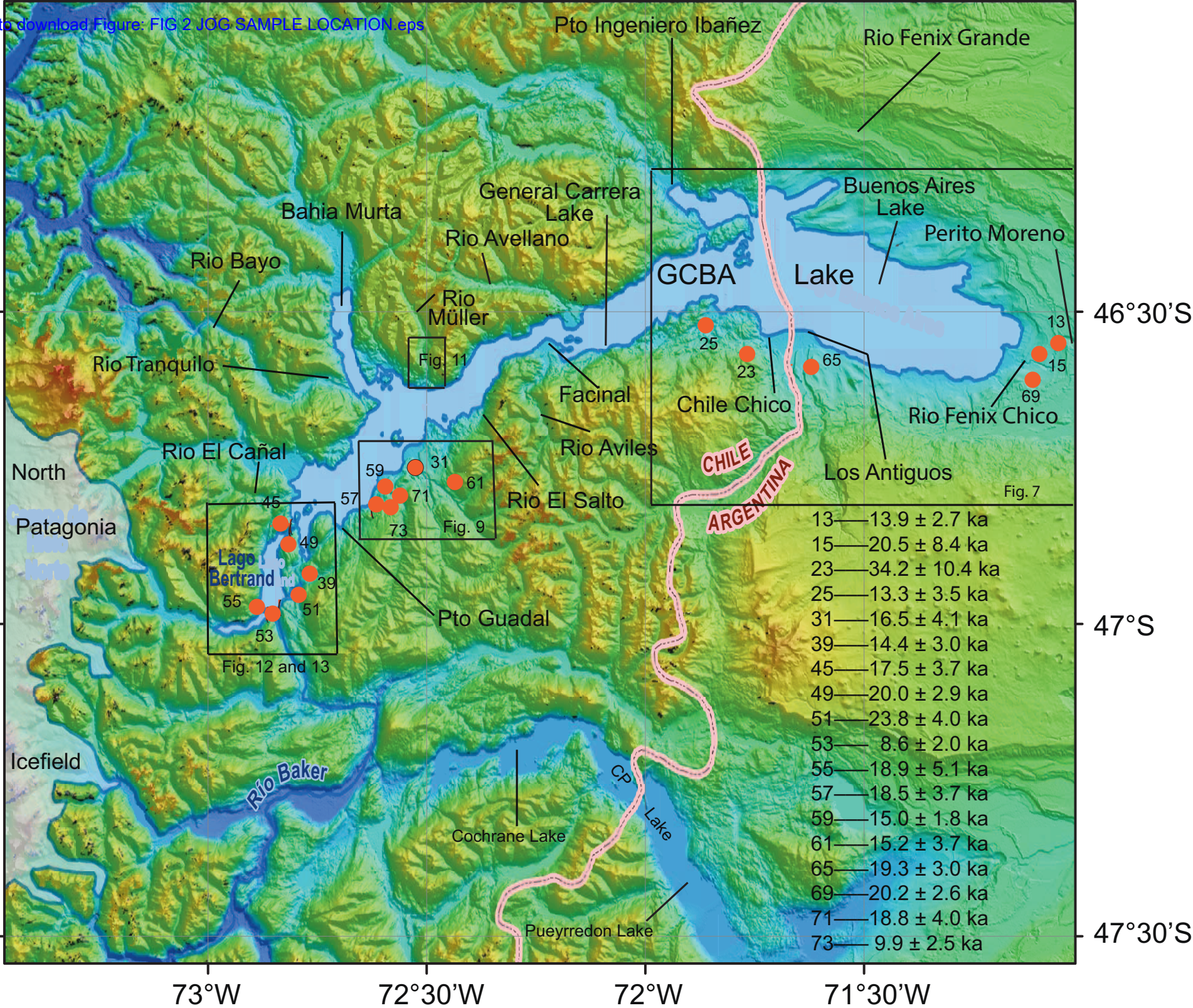




Figure  
[Click here to download Figure: FIG 2 JOG SAMPLE LOCATION eps](#)





Figure

[Click here to download Figure: FIG 3 TERRACES PHOTOS.eps](#)

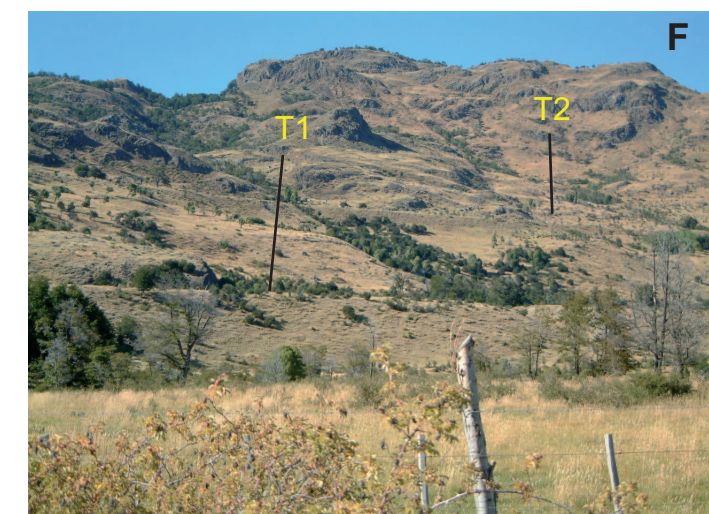
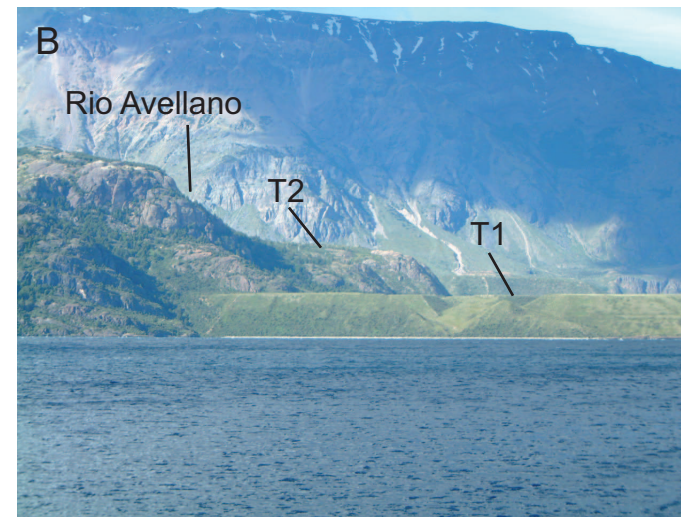
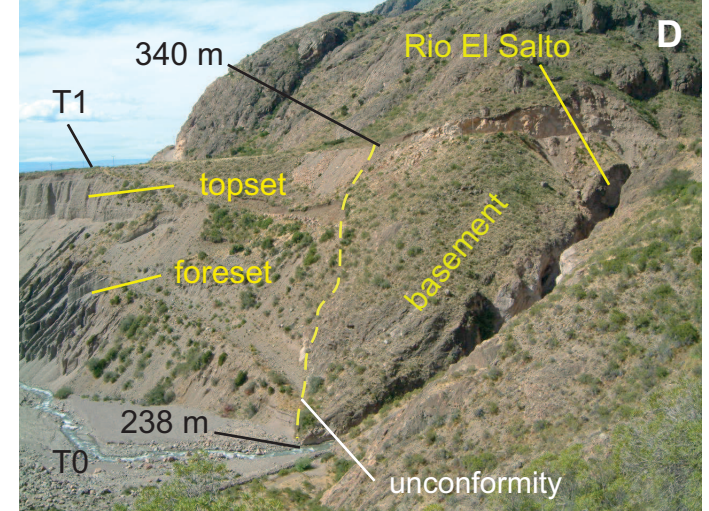
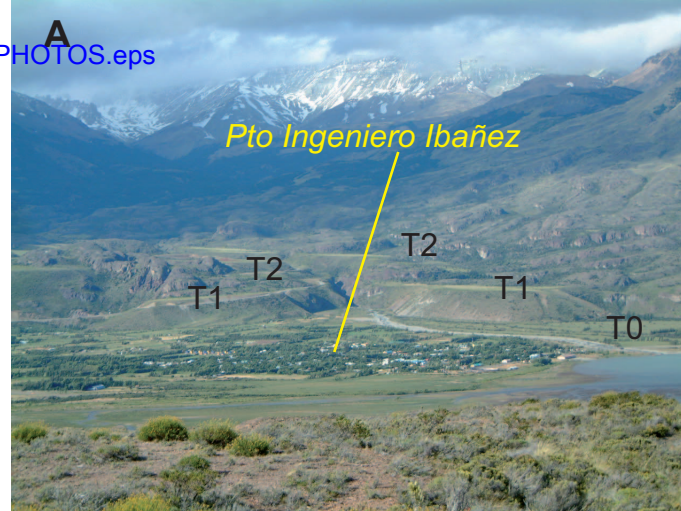




Figure  
[Click here to download Figure: FIG 4 STRANDLINES PHOTOS.eps](#)

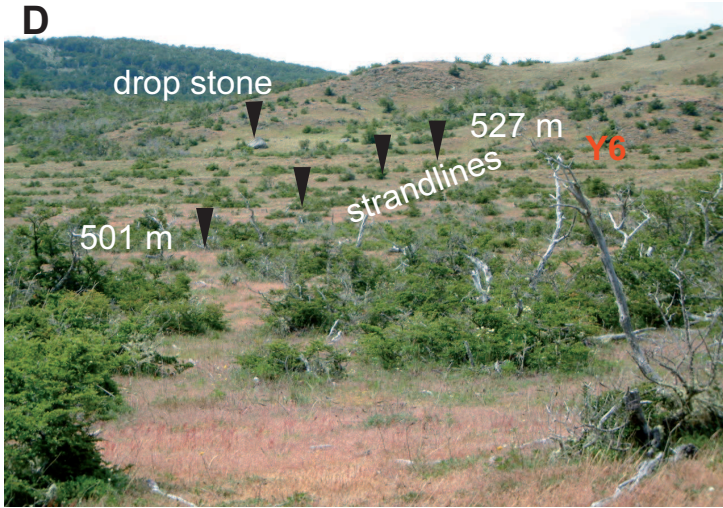
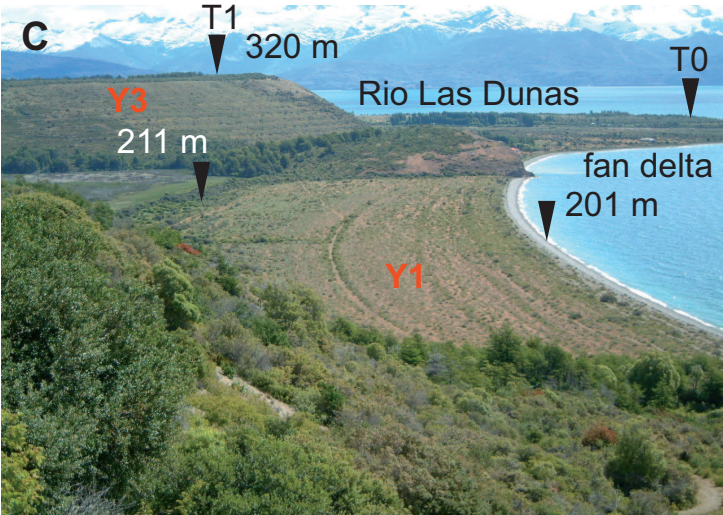
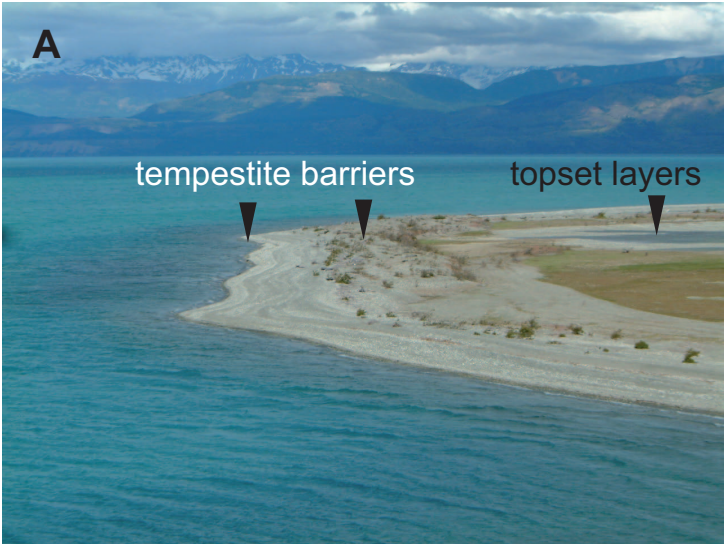








Figure  
Click here to download Figure: FIG 6 CHRONOLO.eps

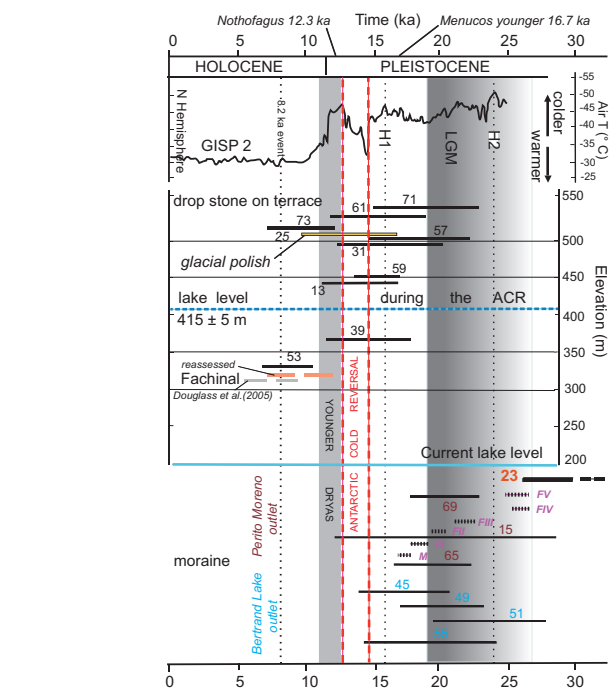


Figure  
[Click here to download Figure: FIG 7 GCBL EAST.eps](#)

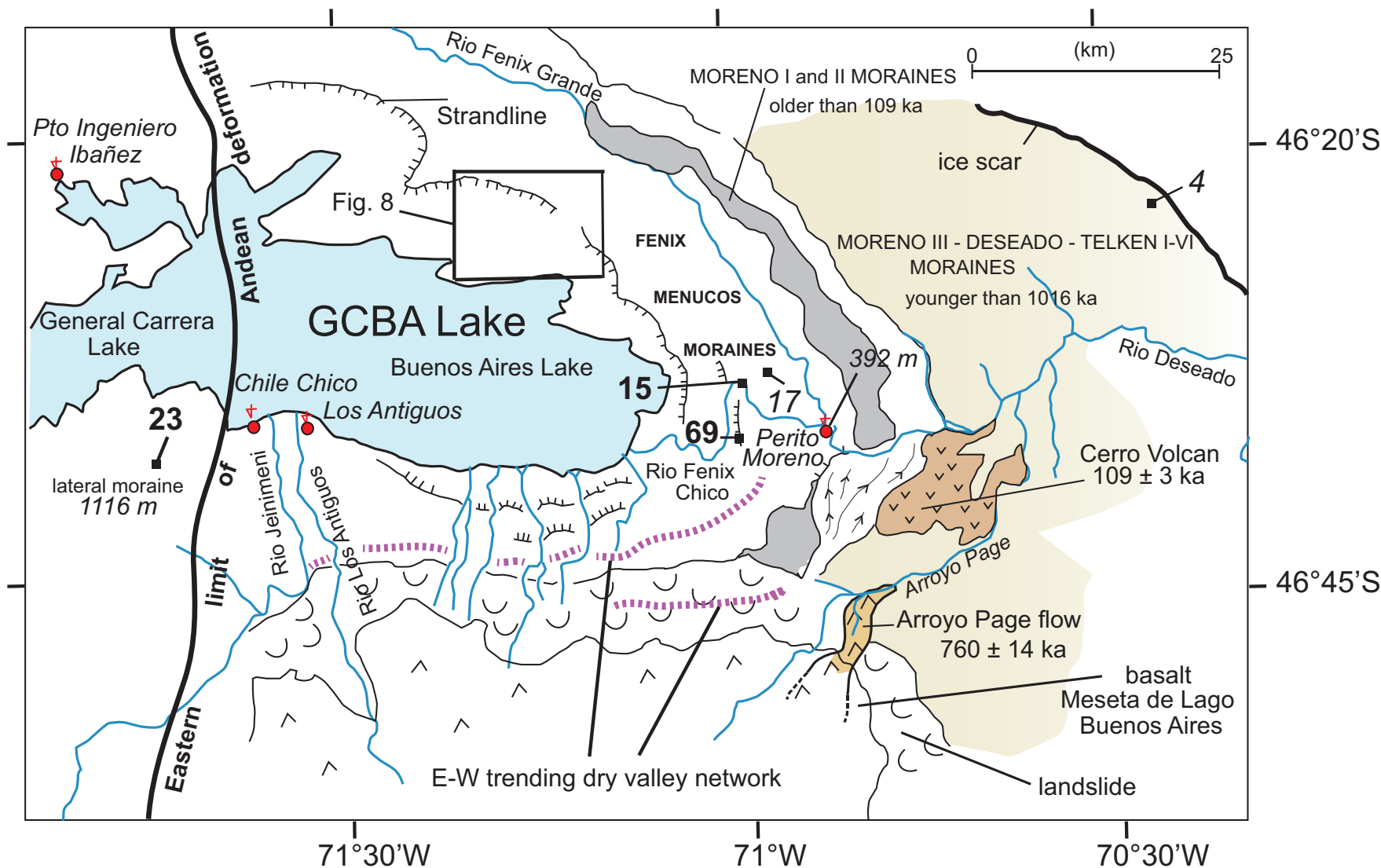




Figure  
Click here to download Figure: FIG 8 BRAIDED PATTERN.eps

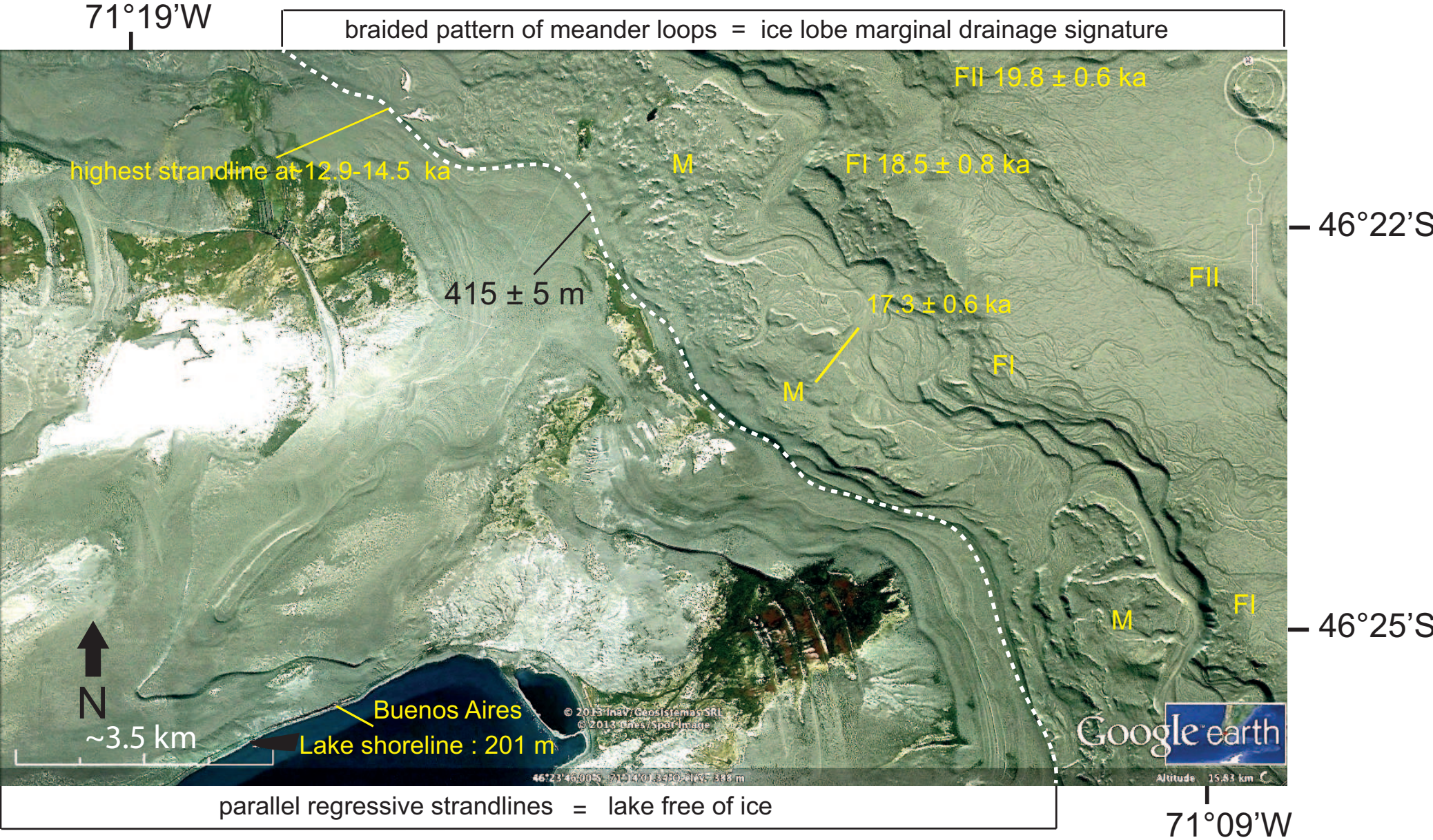




Figure  
[Click here to download Figure: FIG 9 DUNAS.eps](#)

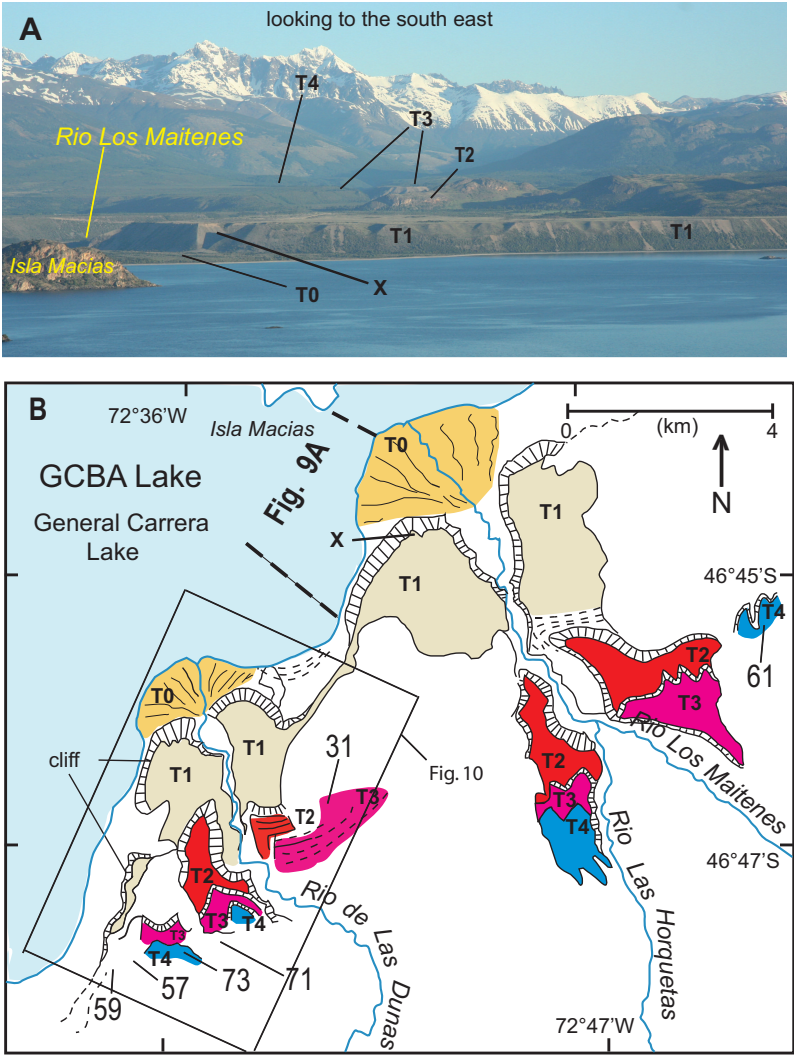


Figure  
[Click here to download Figure: FIG 10 RIO DUNAS.eps](#)

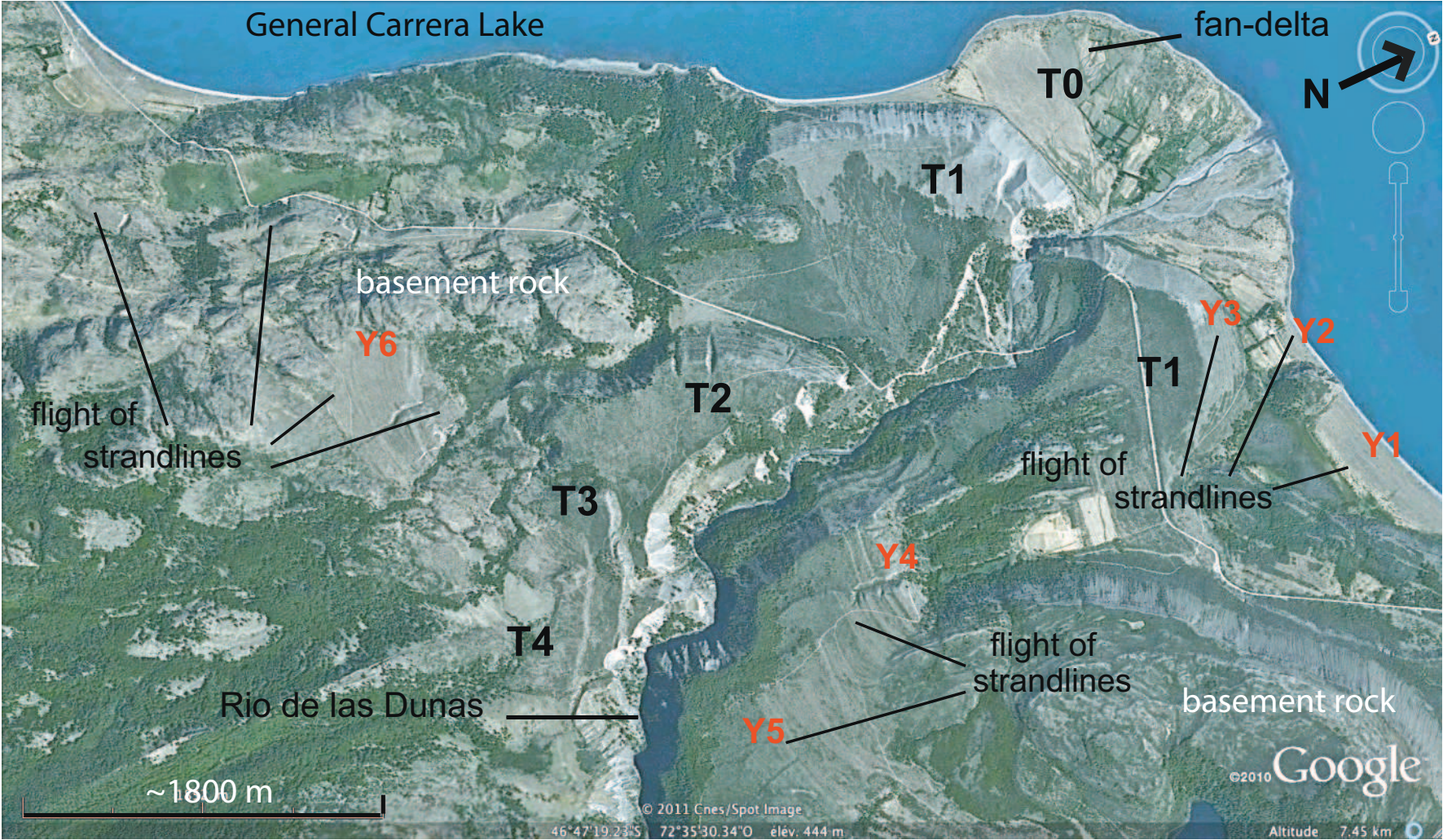




Figure  
[Click here to download Figure: FIG 11 RIO MÜLLER.eps](#)

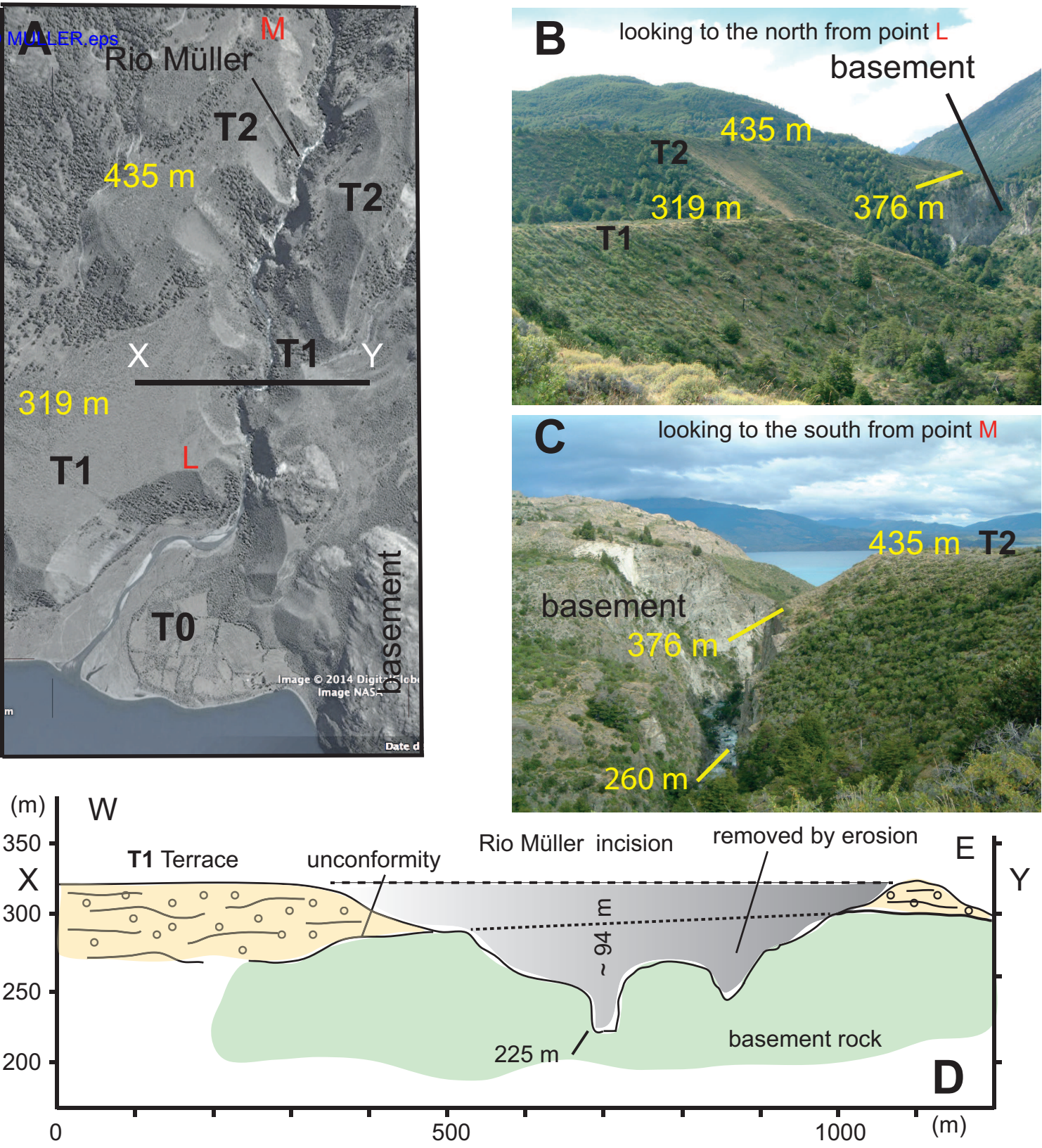


Figure  
[Click here to download Figure: FIG 12 OUTLET BAKER.eps](#)

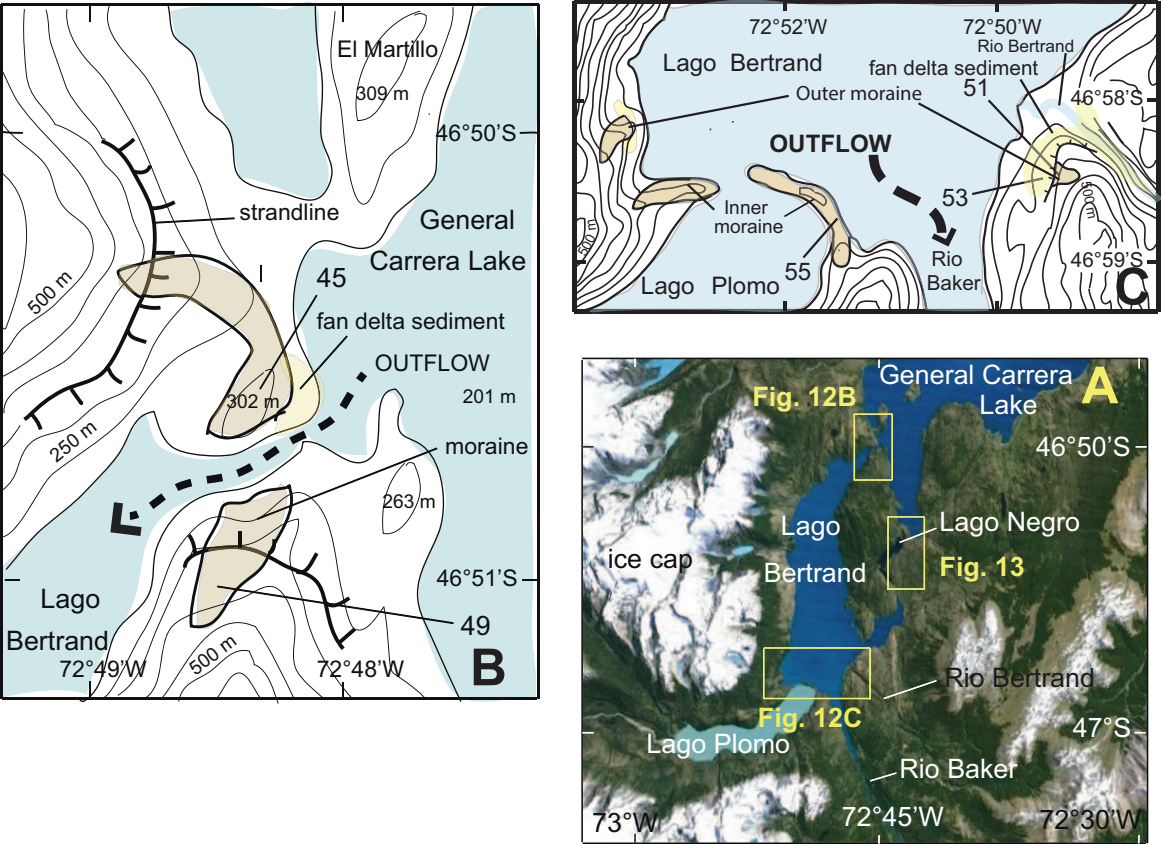




Figure  
[Click here to download Figure: FIG 13 LAGO NEGRO.eps](#)

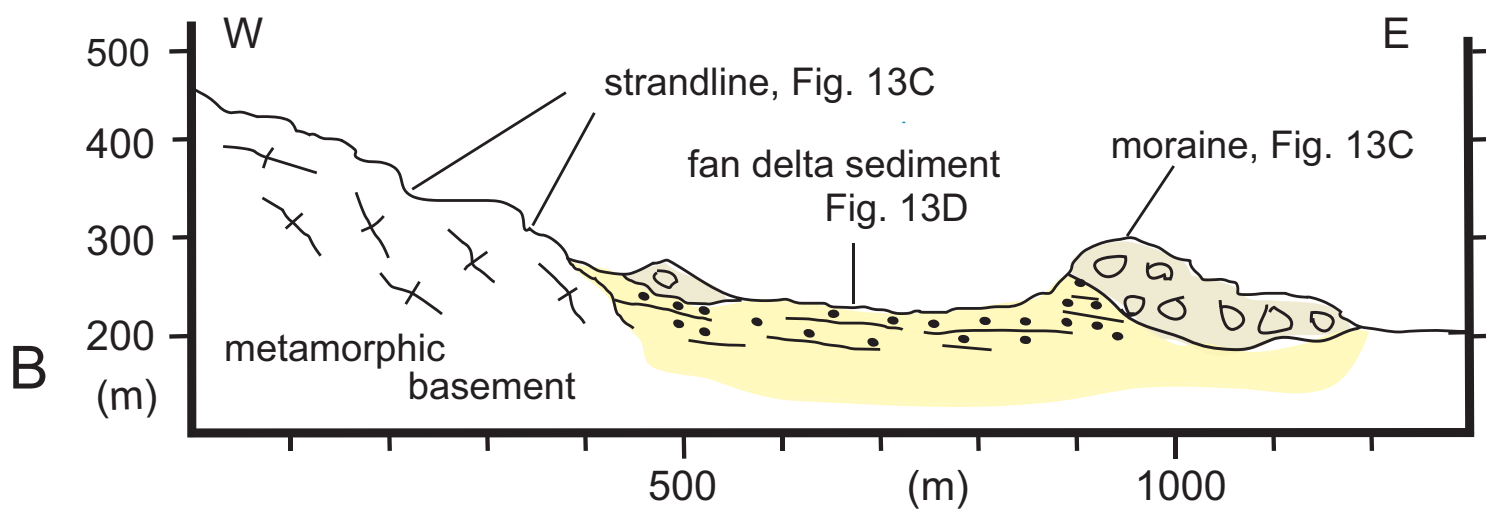
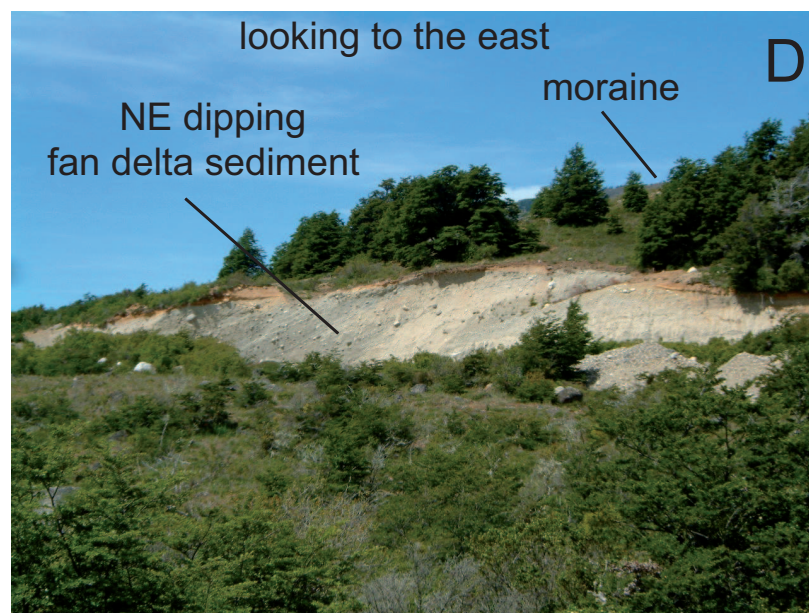
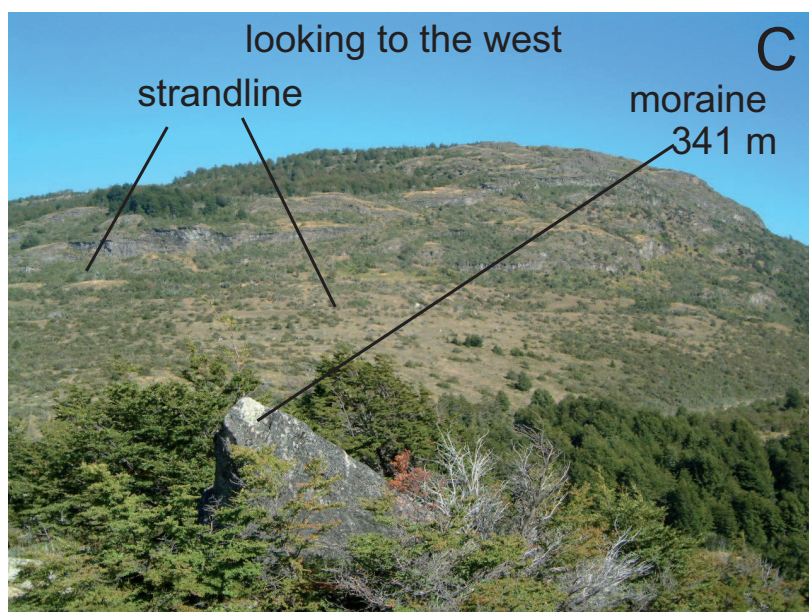
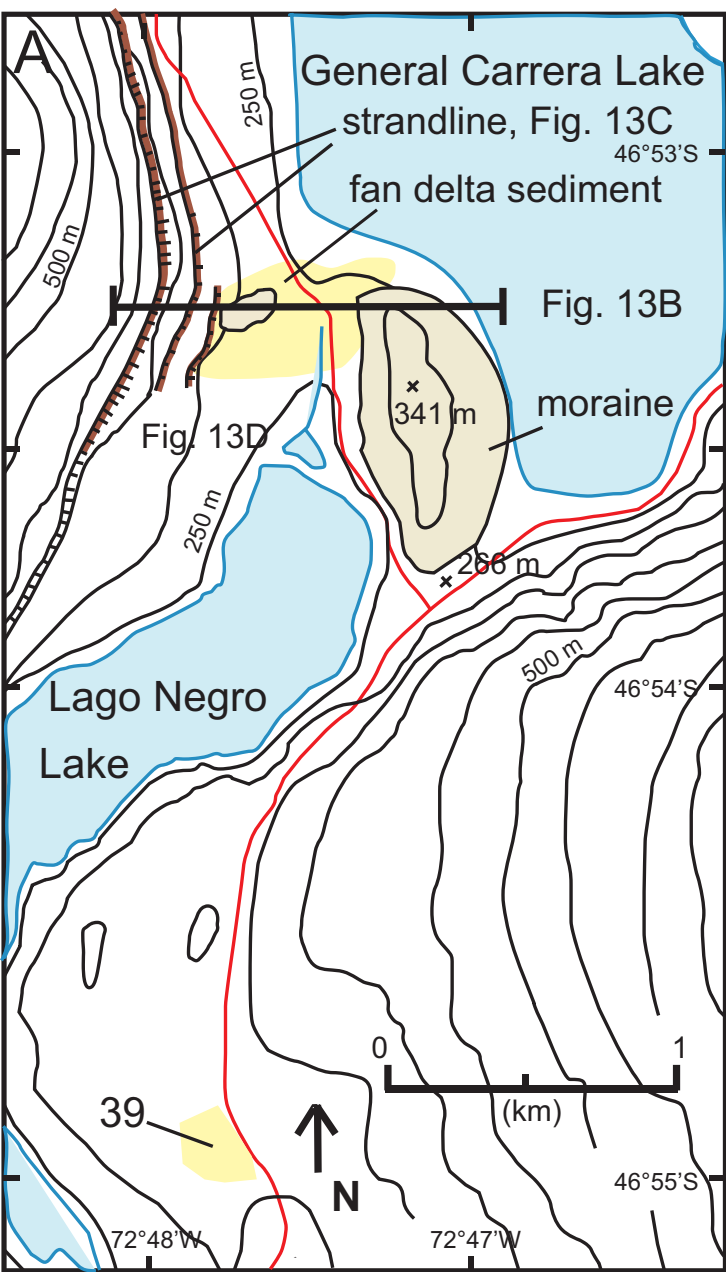


Figure  
[Click here to download Figure: FIG 14 TERRACE CORRELATION.eps](#)

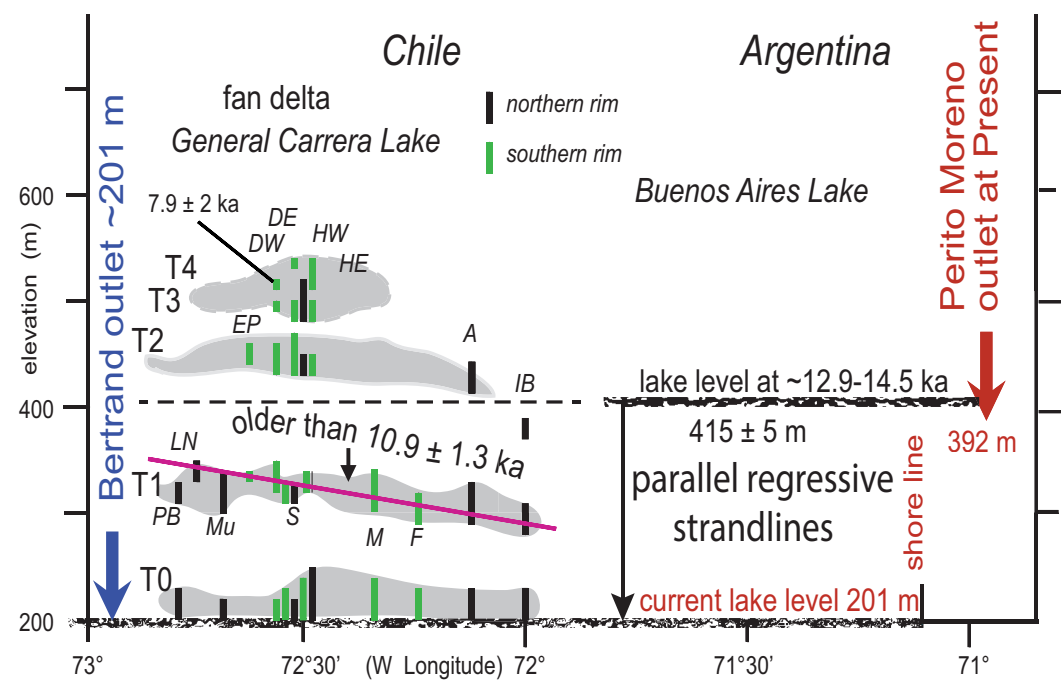
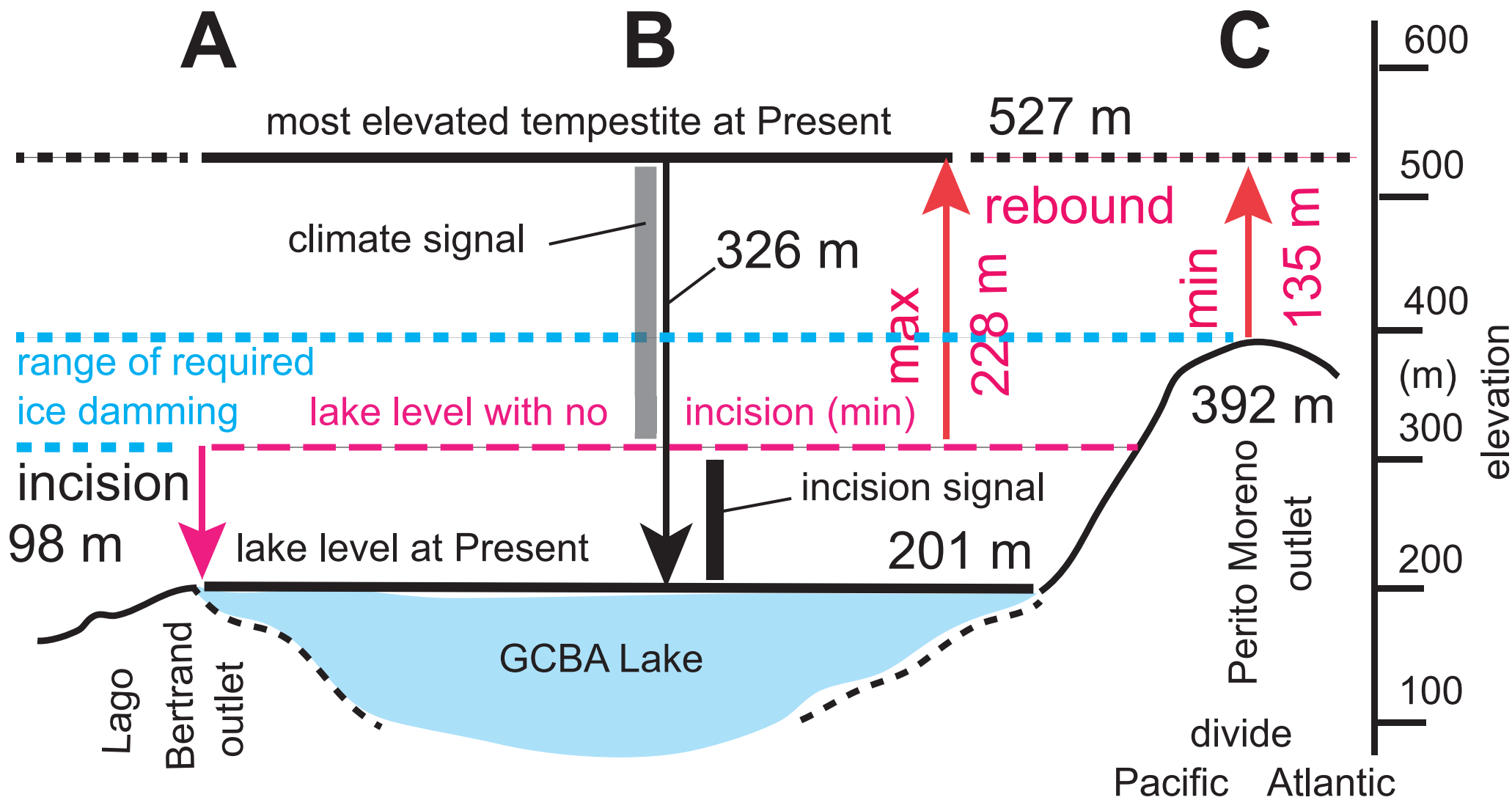


Figure  
Click here to download Figure: FIG 15 REBOUND.eps





Table

Sample number	Sample	Lat (°S)	long (°W)	Elevation (m)	Depth (cm)	Production at/g/yr
4	M	46°24'19.4"	70°29'17.9"	644	1	7.391777778
13	DS	46°31'22.4"	70°57'47.2"	451	2 to 5	6.32288889
15	M	46°32'31.8"	71°02'00.4"	392	2	6.01866667
17	M	46°32'31.5"	71°00'43.0"	449	2	6.314666667
23	M	46°34'52.7"	71°47'28.8"	1116	3	10.70533
25	GP	46°33'29.5"	71°52'02.4"	512	2 to 5	6.64355556
31	DS	46°46'51.1"	72°33'57.5"	494	1	6.63533333
39	DS	46°54'42.2"	72°47'27.4"	364	2	5.887111111
45	M	46°50'24.3"	72°48'19.6"	299	2	5.45955556
49	DS	46°51'01.6"	72°48'29.4"	334	2	5.63222222
51	M	46°58'34.2"	72°49'51.6"	360	3	5.78022222
53	DS	46°58'34.2"	72°50'00.1"	335	3	5.65688889
55	M	46°58'50.5"	72°51'42.0"	290	2 to 3	5.42666667
57	DS	46°48'39.9"	72°36'42.1"	501	2 to 3	6.53666667
59	DS	46°48'38.4"	72°37'19.1"	450	3	6.24888889
61	DS	46°44'45.9"	72°26'55.3"	520	2	6.64355556
65	M	46°39'50.2"	71°36'19.1"	572	2 to 3	6.93133333
69	M	46°35'23.9"	71°02'16.1"	441	2 to 3	6.17488889
71	DS	46°48'16.1"	72°35'19.8"	531	2 to 3	6.70933333
73	DS	46°48'22.0"	72°35'58.1"	521	2 to 3	6.65177778

The top of all samples were exposed at the surface

DS = Drop stone; M = Moraine; GP = Glacial polish

<sup>10</sup> Be at/g	<sup>10</sup> Be error at/g	Tmin (yr)	± 1σ a
5,369,484	228,487	913,185	38,859
84,110	16,382	13,940	2,715
119,441	48,893	20,463	8,377
2,239,409	274,129	401,656	49,167
346 324	104 936	34 164	10 352
84,257	21,902	13,292	3,455
107,858	27,158	16,464	4,145
82,436	17,366	14,414	3,036
92,575	19,502	17,457	3,678
109,328	15,959	20,002	2,920
130,900	22,167	23,774	4,026
46,396	11,024	8,576	2,038
97,701	26,276	18,869	5,075
116,084	23,477	18,472	3,736
89,293	10,789	14,977	1,810
97,818	23,905	15,170	3,707
128,259	19,715	19,258	2,960
119,920	15,649	20,201	2,636
121,023	25,495	18,766	3,953
63,531	15,997	9,914	2,496

Table

Lake shore	W	N + S	N	S	N	S	S	S	S	N	S	N	N	E
Long W	72°50′	72°49′ 72°47′	72°42′ 72°40′	72°38′ 72°35′	72°36′ 72°34′	72°36′ 72°33′	72°35′ 72°34′	72°33′ 72°31′	72°33′- 72°30′	72°31′ 72°29′	72°14′- 72°12′	72°12′ 72°08′	72°03′ 71°56′	70°57′
	LB	PB+LN	Mu	EP	S	DW	DE	HW	Ma	Al	F	A	IB	PM
	fan/stra	stra/fan	fan	stra/fan	Fan	fan	fan	fan	fan	fan	Fan	fan	fan	stra
T4				57 19.1±3.9 501		73 10.1±2.5 527 504	71 19.4±4.1 528 503		61 15.6±3.8 520 499					13 14.3±2.8 451
T3						492 485	31 17.0±4.3 494 472	495 485	494 481					
T2				59 15.4±1.9 452 443		465 433	468 434	458 441	445 432	448 413		413 391	389 370	
T1	53 8.7±2.1 349 335	39 14.8±3.1 329 364 305	334 302	339 331	325 309	347 317	328 316	330 314	342 302	329 294	314 293	326 295	310 281	
T0	201	232 201	222 201	201	228 201	222 201	222 201	238 201	238 201	216 201	225 201	229 201	226 201	